Biomaterials 313 (2025) 122768

Contents lists available at ScienceDirect

Biomaterials

journal homepage: www.elsevier.com/locate/biomaterials

Local delivery of platelet-derived factors mitigates ischemia and preserves ovarian function through angiogenic modulation: A personalized regenerative strategy for fertility preservation

Nanum Chung [a,b], Chungmo Yang [b,e], Heeseon Yang [a,b], Jungwoo Shin [a,b], Chae Young Song [a,b], Hyewon Min [a,b], Ji Hyang Kim [d,***], Kangwon Lee [f,**], Jung Ryeol Lee [a,b,c,*]

[a] Department of Translational Medicines, Seoul National University College of Medicine, Seoul, 03080, Republic of Korea
[b] Department of Obstetrics and Gynecology, Seoul National University Bundang Hospital, Seongnam, 13620, Republic of Korea
[c] Department of Obstetrics and Gynecology, Seoul National University College of Medicine, Seoul, 03080, Republic of Korea
[d] Department of Obstetrics and Gynecology, Fertility Center of CHA Bundang Medical Center, CHA University School of Medicine, Seongnam, 13496, Republic of Korea
[e] Program in Nanoscience and Technology, Graduate School of Convergence Science and Technology, Seoul National University, Seoul, 08826, Republic of Korea
[f] Department of Applied Bioengineering, Graduate School of Convergence Science and Technology, Seoul National University, Seoul, 08826, Republic of Korea

ARTICLE INFO

Keywords:
Fertility preservation
Platelet-rich plasma
Fibrin
Avascular transplantation
Ischemia
Neovascularization
Personalized regenerative medicine

ABSTRACT

As the most prominent and ideal modality in female fertility preservation, ovarian tissue cryopreservation, and transplantation often confront the challenge of ischemic damage and follicular loss from avascular transplantation. To surmount this impediment, we engineered a novel platelet-derived factors-encapsulated fibrin hydrogel (PFH), a paradigmatic biomaterial. PFH encapsulates autologous platelet-derived factors, utilizing the physiological blood coagulation cascade for precise local delivery of bioactive molecules. In our study, PFH markedly bolstered the success of avascular ovarian tissue transplantation. Notably, the quantity and quality of follicles were preserved with improved neovascularization, accompanied by decreased DNA damage, increased ovulation, and superior embryonic development rates under a Low-concentration Platelet-rich plasma-derived factors encapsulated fibrin hydrogel (L-PFH) regimen. At a stabilized point of tissue engraftment, gene expression analysis mirrored normal ovarian tissue profiles, underscoring the effectiveness of L-PFH in mitigating the initial ischemic insult. This autologous blood-derived biomaterial, inspired by nature, capitalizes on the blood coagulation cascade, and combines biodegradability, biocompatibility, safety, and cost-effectiveness. The adjustable properties of this biomaterial, even in injectable form, extend its potential applications into the broader realm of personalized regenerative medicine. PFH emerges as a promising strategy to counter ischemic damage in tissue transplantation, signifying a broader therapeutic prospect. (***197 words***)

1. Introduction

Today, our world has seen impressive progress in medicine, engineering, and science, driving significant economic and social change. This has resulted in a rise in life expectancy to around 100 years, better survival rates for diseases like cancer, and increased gender-neutral social participation [1]. These changes have increased the need for fertility preservation (FP) among cancer survivors and those delaying family planning, highlighting its significance. FP, with advanced technologies, improves lives today and addresses global birth rate decline [2,3].

Female FP methods like oocyte, embryo, and ovarian tissue (OT) cryopreservation and transplantation (OTC and OTT) are widely employed [1–4]. OTC and OTT are crucial methods for pediatric, emergent, single, and peri/post-menopausal patients [3–5]. In 2020, about 200 successful live births resulted from OTC and OTT [6]. Still, challenges exist in the process. Cryo-damage in OTC was a concern, but improved vitrification-warming techniques and materials have greatly reduced it [7–11]. Ovarian follicle survival after tissue grafting depends

* Corresponding author. Department of Obstetrics and Gynecology, Seoul National University College of Medicine, Seoul, 03080, Republic of Korea.
** Corresponding author.
*** Corresponding author.
E-mail addresses: bin0902@chamc.co.kr, bin080902@gmail.com (J.H. Kim), kangwonlee@snu.ac.kr, kangwonl@gmail.com (K. Lee), leejrmd@snu.ac.kr, leejrmd@gmail.com (J.R. Lee).

https://doi.org/10.1016/j.biomaterials.2024.122768
Received 19 June 2024; Received in revised form 11 August 2024; Accepted 20 August 2024
Available online 30 August 2024

Abbreviations

ACD Anticoagulant Cirtate Dextrose
Ang-1 Angiopoietin-1
ANOVA Analysis of Variances
ARES Advanced Rheometric Expansion System
Bax B-Cell Leukemia/Lymphoma 2 (Bcl2) Associated X
bECM Basal Endothelial Cell Medium
C.B.C. Complete Blood Count
CCL-2 C–C Motif Chemokine Ligand 2
CD26 Cluster of Differentiation 26
CD31 Cluster of Differentiation 31
cDNA Complementary Deoxyribonucleic Acid
COCs Cumulus-Oocyte complexes
CXCL-16 C-X-C motif chemokine ligand 16
DAPI 4′,6-Diamidino-2-Phenylindole, dihydrochloride
DNA Deoxyribonucleic Acid
DPBS Dulbecco's Phosphate Buffered Saline
ECM Extracellular Matrix
FBS Fetal bovine serum
FH Fibrin Hydrogel
FH-O Fibrin Hydrogel-only
FP Fertility Preservation
FSH Follicle Stimulating Hormone
Fshr Follicle Stimulating Hormone Receptor
G1, G2, G3 follicles Grade 1, 2, and 3 follicles
Gapdh Glyceraldehyde-3-phosphate dehydrogenase
GCs Granulosa cells
H&E Hematoxylin and Eosin
hCG Human Chorionic Gonadotropin
HGF Hepatocyte Growth Factor
H-PFH(D) Derivatives of High-concentration Platelet-rich plasma-derived factors encapsulated fibrin hydrogel
H-PFH High-concentration Platelet-rich plasma-derived factors encapsulated fibrin hydrogel
H-PRP High-concentration Platelet-rich plasma
HTF Human tubal fluid
HUVECs Human Umbilical-cord Vein Endothelial Cells
IGFBP Insulin-like Growth Factor Binding Protein
IHC, IHC-P Immunohistochemistry, Immunohistochemistry-paraffin-embedded
IVF *In vitro* Fertilization
IVM *In vitro* Maturation
Lhcgr Luteinizing hormone/chorionic gonadotropin receptor
L-PFH(D) Derivatives of Low-concentration Platelet-rich plasma-derived factors encapsulated fibrin hydrogel
L-PFH Low-concentration Platelet-rich plasma-derived factors encapsulated fibrin hydrogel
L-PRP Low-concentration Platelet-rich plasma
MII Metaphase II
MMP Matrix Metalloproteinase
n Number
O/N Overnight
OPN Osteopontin
OTC Ovarian Tissue Cryopreservation
OTs Ovarian Tissues
OTT Ovarian Tissue Transplantation
PAI-1 Plasminogen Activator Inhibitor-1
PDGF-AA, AB/BB Platelet-derived Growth Factor-AA, and -AB/BB
PEDF Pigment Epithelium-Derived Factor
PF4 Platelet Factor 4
PFH Platelet-derived Factors-Encapsulated Fibrin Hydrogel
PFs Platelet-derived Factors
PlGF-2 Placental Growth Factor-2
PMSG Pregnant Mare Serum Gonadotropin
PPP Platelet-poor plasma
PRF Platelet-rich fibrin
PRP Platelet-rich plasma
PS Penicillin-streptomycin
PTX-3 Pentraxin-3
qRT-PCR Quantitative Realtime-polymerase Chain Reaction
RBCs Red Blood Cells
RNA RiboNucleic Acid
RT Room Temperature
RT-PCR Reverse Transcriptase-polymerase chain reaction
SD Standard Deviation
SEM Scanning Electron Microscopy
TCs Theca cells
TIMP Tissue Inhibitor of Metalloproteinase
TSP-2 Thrombospondin-2
TUNEL Terminal deoxynucleotidyl transferase dUTP nick-end labeling
w/, w/o with, without
WB Whole Blood

on precise timing and the right proangiogenic factors, crucial for rapid revascularization post-transplantation [12]. Tissue survival varies significantly based on the transplant site and microenvironment disparities [13,14]. Unfortunately, a considerable follicle loss occurs before full graft revascularization, affecting a significant portion of the reserve, estimated at 50 %–90 % [15,16]. Today, ischemia-induced ovarian damage is the main factor compromising FP effectiveness with OTs [17]. Studies address follicle loss with approaches such as administering angiogenic factors, stem cells, antioxidants, and anti-apoptotic drugs during OTTs across different species, including human xenografts [18–23]. Despite showing potential for vascular formation and inflammation control, cell-based therapies remain contentious regarding safety, primarily due to concerns over potential cancerogenesis stemming from unanticipated cell differentiation and proliferation, variability in therapeutic outcomes based on cell origin, and inherent instability, posing significant challenges for their clinical implementation [24]. Yet, these methods pose a risk of cancer recurrence and may harm nearby follicles when directly injected into the OT. Safe strategies are urgently needed to prevent ischemic injury and optimize avascular OT transplantation [25–27].

Platelet-rich plasma (PRP), from venous blood, contains bio-reactive molecules like growth factors, cytokines, and chemokines [28–30]. PRP is established in plastic surgery, orthopedics, and dentistry for its safety, simplicity, and efficacy [31–33]. PRP shows promise in FP, with intra-ovarian or intrauterine injection improving reproductive dysfunction. Despite progress, PRP's exact mechanism on women's reproductive organs remains unclear [34–41].

Fibrin, a natural polymer from fibrinogen and thrombin cross-linking, plays a crucial role in blood coagulation and serves as a biomedical hydrogel. It attaches cells, supports growth factors, and allows sustained release. Research using fibrin hydrogel (FH) exclusively shows promise, improving wound healing, tissue regeneration, and reducing complications due to its natural origin and biocompatibility [42–45]. Platelet activation in PRP happens when exposed to the extracellular matrix, fibrin clot, thrombin, and calcium ions, releasing potent molecules akin to blood coagulation [46,47].

Therefore, we hypothesized that platelet-derived factors and PFH, produced by applying various factors and the blood coagulation mechanism, could reduce ischemic damage, thereby increasing tissue survival and follicle preservation. In other studies that compared cell

proliferation and survival in vitro by varying the concentration of PRP after activation, relatively lower concentrations yielded more effective results. They discussed that the reason relatively lower concentrations were more effective is due to differences in factors released from alpha granules during PRP activation, leading to a relatively reduced inflammatory response [47]. Hence, in this study, we designed experiments to investigate the varying effects of PRP-derived factors depending on concentration and the reasons behind these differences.

To expedite revascularization and protect against ischemia in OTT, we developed "Platelet-derived factor-encapsulated Fibrin Hydrogel (PFH)" by combining PRP and FH. Our hypothesis is that PFH can reduce ischemic tissue failure, benefiting both the recipient and transplanted ovaries. This has the potential to enhance tissue repair, safeguard follicles, promote recovery, and angiogenesis. We speculate that the composition and concentration of platelet-derived factors (PFs) can impact neovascularization and vessel maturation. By exploring PFH's potential, we aim to improve OTT and fertility preservation strategies.

2. Materials and Methods

2.1. Experimental design

Six to eight-week-old B6D2F1 mice were divided into five groups: fresh, sham, fibrin hydrogel-only (FH–O), low-concentration Platelet-rich plasma (L-PRP)-derived factors encapsulated fibrin hydrogel (L-PFH), and high-concentration Platelet-rich plasma (H-PRP)-derived factors encapsulated fibrin hydrogel (H-PFH). L-PRP and H-PRP samples were prepared and assessed for angiogenic potential and bioactive factor content before surgery. Etulain et al. compared the effects of PRP at concentrations of 0 %, 5 %, 10 %, 25 %, 50 %, 75 %, and 100 %. They reported that a 25 % concentration of PRP demonstrated superior effects on cell proliferation and survival compared to the commonly used 100 % concentration. Therefore, in this study, we established a low-dose group, diluted to 1/4, to compare its effects with clinically used PRP (100 %, High) [47]. In this study, 10 mice per group were used in experiments for histological and molecular assessments. For in vitro fertilization, 18 mice were used per batch. Additionally, for the preparation of PRP, a total of 90 animals were used, with 30 animals each in 3 repeated experiments. On the day of transplantation, ovaries were encapsulated according to their respective group protocols and auto-transplanted subcutaneously into the dorsal region. To verify the protective effect of PFH more effectively against ischemic damage, we chose the method that induces the greatest ischemic damage. This approach is based on the ovarian ischemic damage model described in a previous publication [48]. The researchers compared the extent of ischemic damage when ovarian tissue was transplanted into different locations, including subcutaneously, under the kidney capsule, into adipose tissue, and into muscle tissue. The results showed that subcutaneous transplantation induced the most severe ischemic damage. Following transplantation, right-sided ovarian grafts were collected at intervals of 1, 3, 7, and 21 days, fixed in 4 % paraformaldehyde for histological examination. Left-sided ovarian grafts were stored at −80 °C for gene expression analysis. Superovulation, oocyte retrieval, in vitro maturation (IVM), in vitro fertilization (IVF), and gene expression analysis were performed 21 days post-transplantation, coinciding with the typical stabilization of graft vascularization and engraftment [45]. Detailed specifications and preparations for PRP, Gel base (A), and Activator (B) can be found in the Materials and Methods section (Fig. 1).

2.2. Ethics approval and consent to participate

This study utilized 6–8-week-old B6D2F1 female mice from Orient Co. (Seongnam, Korea) and housed them in ventilated cages under controlled temperature, humidity, and light conditions, with free access to food and water. All procedures followed ethical guidelines established by the Institutional Animal Care and Use Committee of Seoul National University Bundang Hospital (Approval number: BA1801-240/009–01). Anesthetics Zoletil and Rompun were used in compliance with permissions granted by the Korea Food and Drug Administration for controlled substances in academic research (Approval Number: Gyeongin No. 706). The study did not involve human subjects.

2.3. Preparation of allogenic mouse L-PRP, H-PRP, L-PFH, and H-PFH and their derivatives (L-PFH(D), and H-PFH(D))

The female mice underwent anesthesia using a mixture of Zoletil® 50 (Virbac, Korea) and Rompun® (Xylazine injection, Dechra Veterinary Products, USA). Whole blood (WB) was collected via cardiac puncture from each mouse using a 1 mL syringe preloaded with anticoagulant citrate dextrose (ACD) solution (Huons, Seongnam, Korea) at a 9:1 blood-to-ACD ratio. The collected samples were transferred to a PRS™ BIO KIT (Prodizen Inc., Seoul, South Korea) and centrifuged at 3500 rpm for 7 min at room temperature (22–26 °C; RT) with gradual deceleration. PRP, containing the buffy coat layer, a small volume of red blood cells (RBCs), and platelet-poor plasma (PPP), was separately collected using 1-mL and 10-mL syringes. Approximately 250–300 μL of PRP was mixed with 2 mL of PPP through a syringe connector to create H-PRP. This H-PRP was further diluted by a quarter in PPP to produce L-PRP and stored at −20 °C for future use. Platelet concentrations in WB, PPP, and H-PRP were measured via a complete blood count (C.B.C.; HEMAVET® 950, Drew Scientific, Oxford, UK). The PFH of L-PRP and H-PRP were prepared by mixing them with Gel base (A) solution (Fibrinogen, Aprotinin, and L- or H-PRP) and then adding the Activator (B) solution (Thrombin and Calcium chloride ($CaCl_2$)). After 30 min of incubation at RT, the polymerized gels were designated as L-PFH and H-PFH. To obtain derivatives (D) from L- and H-PFH, centrifugation was performed at 14,000 rpm, 4 °C, for 20 min. The supernatant of each gel was designated as L-PFH(D) and H-PFH(D), respectively.

2.4. In vitro and ex vivo angiogenic potential assays of L-PFH(D) and H-PFH(D)

To evaluate and compare the angiogenic potential of PPP, L-PFH(D), and H-PFH(D), we performed tube formation and aortic ring assays. For the in vitro tube formation assay, Human Umbilical-cord Vein Endothelial Cells (HUVECs; Promocell, Heidelberg, Germany) were utilized. Each well of a 48-well culture plate was coated with 200 μL/well of Matrigel® Matrix (Growth factor-reduced, Corning, NY, USA) and incubated at 37 °C for 30 min. Subsequently, 5×10^4 cells/well were seeded and cultured in basal Endothelial Cell Medium (bECM; ScienCell, Carlsbad, USA) without growth factor supplementation, with or without the L- and H-PFH derivatives. After a 12-h incubation, branching points were quantified using Image J software (National Institutes of Health, Bethesda, MD, USA). For the *ex vivo* aortic ring assay, whole abdominal aortas from four B6D2F1 mice were harvested, cleared of surrounding connective tissues, and cut into 1 mm segments under microscopic observation. Each well of a 48-well culture plate was pre-coated with 200 μL/well of Matrigel® Matrix (Growth factor-reduced, Corning, NY, USA) and incubated at 37 °C for 30 min. The trimmed aortic rings were placed at the center of each well, completely covered with 100 μL/well of Matrigel® Matrix and incubated at 37 °C for 30 min. We then added basal ECM medium (without supplementation) with either Dulbecco's phosphate-buffered saline (DPBS; WelGENE Inc., Korea) or the L- and H-PFH derivatives, following the same protocol as the tube formation assay. After a 4-day incubation, emerging sprouts were quantified using the same methods.

2.5. Proteome profiling of platelet-derived bioactive molecules in L-PFH (D) and H-PFH(D)

To analyze platelet-derived constituents, we conducted angiogenesis-associated proteome screening using a Mouse

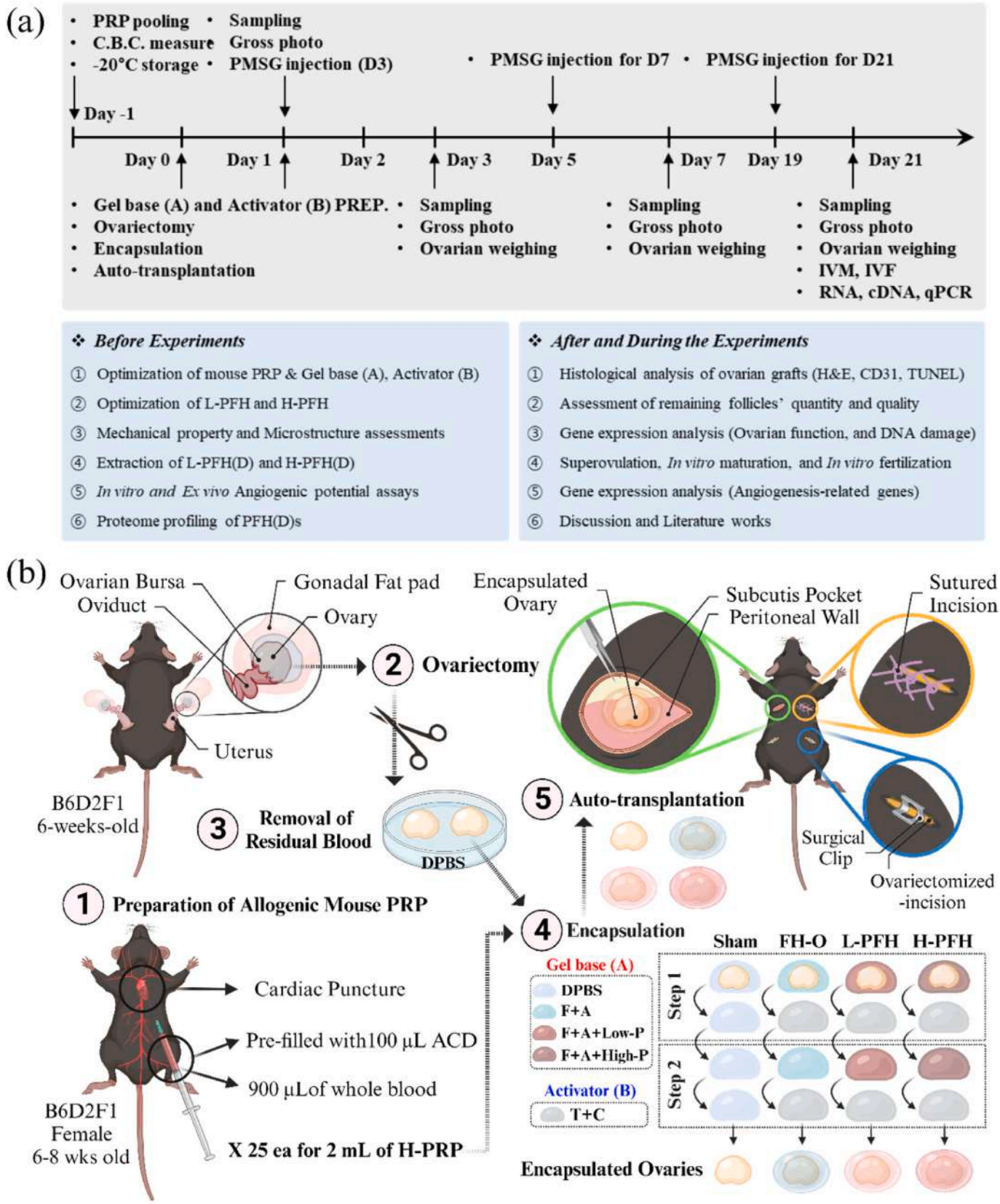

Fig. 1. Schematic illustration of experimental timeline and design. (a) Study timeline. Prior to experimentation, materials were optimized and characterized. Subsequent procedures followed this timeline to validate our hypothesis. (b) Encapsulation procedure schematic. Procedure ① was conducted pre-ovariectomy, encapsulation, and transplantation, while steps ② to ⑤ occurred concurrently on the day of surgery (Created with BioRender.com).

Angiogenesis Proteome Profiling Kit (Proteome Profiler Antibody Arrays, R&D Systems, USA). PPP was prepared for immediate use, and L- and H-PFH(D) were prepared as described earlier, following the same protocol used for ovarian encapsulation with each PFH in this study. After a 30-min activation, L- and H-PFH(D) were centrifuged, and the supernatants were collected and transferred to fresh 1.5 mL tubes for further analysis. PPP, L-, and H-PFH(D) were grouped together for this experiment. The pixel density of each detected proteome was manually quantified using Image J software, following the manufacturer's guidelines, and compared among all groups.

2.6. Fabrication and characterization of FH-O, L-PFH, and H-PFH, and encapsulation process of the ovary

FH-O, used for ovarian encapsulation, was prepared by mixing fibrinogen (5 mg/mL, Sigma Aldrich) and aprotinin (150 KIU/mL, Sigma Aldrich) with thrombin (5 IU/mL, Sigma Aldrich) and a calcium chloride solution (1 mM, Sigma Aldrich). Initially, a 'Gel Base (A)' was created by dissolving fibrinogen and aprotinin in distilled water. For L- and H-PFH preparation, L- and H-PRP were mixed into this Gel Base (A). The 'Activator (B)' was formulated by combining thrombin and $CaCl_2$ solution. The process of whole ovary encapsulation involved immersing the ovaries in DPBS immediately after ovariectomy to remove residual blood, followed by complete immersion in Gel Base (A) and Activator (B), each for 20 s. The drop volume was 20 μL. The storage modulus (G′), loss modulus (G″), and tan(d) of FH-O, L-PFH, and H-PFH were measured under varying strain using an Advanced Rheometric Expansion System (ARES; Rheometric Scientific, UK). Samples were prepared following the same protocols as the encapsulation procedure and placed in a 48-well culture plate. The ARES was maintained at a constant temperature of 37 °C. Samples were positioned between parallel cassettes with an 8 mm diameter, and strain varied from 1 to 300 %. The experiment was conducted at a controlled frequency of 1.0 rad s-1. Subsequently, each gel sample underwent a three-day lyophilization and platinum sputter-coating before evaluating its microstructure using Scanning Electron Microscopy (SEM; SNE-3200, SEC, Suwon, Korea).

2.7. Macroscopic evaluation of ovarian grafts and weighing after hormonal trigger to evaluate the recovery of endocrine function and intact vascularization

Macroscopic evaluation of grafts was conducted before sampling on each observation day. Mice were euthanized by cervical dislocation, and dorsal skin was dissected along the spine. Skin flaps were then carefully arranged on surgical pads for visual assessment of grafts and surrounding vascular structures. Gross images were captured using an iPhone XR camera with a scaling ruler beneath each sample. The weight of ovarian grafts in each group was measured after intraperitoneal administration of 7.5 IU/150 μL/head of pregnant mare serum gonadotropin (PMSG; Prospec, Rehovot, Israel) 48 h before sampling at 3-, 7-, and 21-days post-OTT. On each sampling day (except day 1), before ovulation, grafts were retrieved and weighed using an electronic balance (Adam Equipment Inc., Danbury, CT, USA). The weight gain recovery, influenced by hormonal response, serves as an indicator of intact vessel formation, facilitating successful hormone delivery to the grafts.

2.8. Preparing samples for the histological analysis

Ovarian grafts from the right side of each mouse were collected at 1-, 3-, 7-, and 21-days post-transplantation, fixed in 4 % paraformaldehyde, and incubated overnight at 4 °C. Subsequently, the grafts were paraffin embedded. Tissue slides, with a thickness of 4 μm, were serially sectioned (Microtome Rotary, Leica). Slides at regular intervals (100–150 μm) were chosen for hematoxylin and eosin (H&E) staining (Cancer Diagnostics, Durham, UK) to assess ovarian follicle quantity and quality. Additional sections were used for immunohistochemistry-paraffin-embedded (IHC–P) analysis to detect vascular endothelial cells through Cluster of Differentiation 31 (CD31; Abcam, Cambridge, MA, USA) staining. The terminal deoxynucleotidyl transferase-mediated deoxy-uridine triphosphate nick-end labeling (TUNEL) assay for DNA fragmentation was conducted using the Cell Death Detection Kit (Roche, Mannheim, Germany). Slides for IHC-P and TUNEL assays were selected, deparaffinized, and rehydrated following the same process as the H&E staining in each experimental condition.

2.9. Assessment of quantity and quality of remaining ovarian follicles

Unstained slides were heated to 60 °C for at least 4 h, followed by deparaffinization and rehydration in pure xylene (DAEJUNG, Korea) for 3 cycles of 10 min each and sequential dilutions of ethanol (100, 95, 90, 85, 80, 70, and 50 %) (EMSURE, Merck, Darmstadt, Germany) for 5 min each. The slides were then immersed in hematoxylin for 1 min, rinsed in fresh tap water, dipped in 70 % ethanol containing hydrochloric acid for 3 s, and subsequently placed in eosin for 20 s. After another tap water rinse, the slides were briefly dipped in xylene for 1 s and mounted using Dako Mounting medium (Dako, Copenhagen, Denmark). To assess the remaining follicles in retrieved OTs, H&E-stained slides were examined under a light microscope (Nikon, Tokyo, Japan) at 20X (Secondary and Antral follicles) and 40× (Primordial and Primary follicles) magnifications. Follicles were categorized into four developmental stages based on standard appearances: primordial (single layer of flattened pre-granulosa cells), primary (single-layer granulosa cells (GCs) including cuboidal forms), secondary (at least two layers of cuboidal GCs), and antral (multiple layers of cuboidal GCs with a fluid-filled antrum) [48]. Follicle quality was graded using predefined criteria: Grade 1 (G1) for intact spherical follicle and oocyte, Grade 2 (G2) for detached granulosa cells with a healthy oocyte, and Grade 3 (G3) for disruption of granulosa and theca cells, pyknotic nuclei, and missing oocytes [49]. The results were obtained from the analysis of a total of 10 ovaries per group, with each dot on the graph representing one ovary (as stated in the legend of Fig. 6, d). As we employed the same method as previous literature [48, 49], no separate analysis was conducted for density. Following the methodology outlined in the reference, we conducted a histopathological comparison of follicles within the whole ovary. The slides serially sectioned at 4 μm intervals were chosen at 100 μm intervals for staining, and this procedure was carried out uniformly across all groups to analyze the entire ovary. Analysis was conducted based on criteria from the previous study [48] for all groups, presenting results for total follicle count, stage-wise follicle count and ratio, and Grade 1 follicle count and ratio [49].

2.10. Immunohistochemical staining of CD31 for detecting vascular endothelial cells in ovarian grafts

Immunostaining of Cluster of Differentiation 31 (CD31) in the ovarian grafts was performed to assess blood vessel intensity. After deparaffinization and rehydration, slides were microwave-boiled in target antigen retrieval solution (pH 6.0, citrate buffer, MOSAICON, Korea) for 20 min. Sections were then treated with peroxidase blocking solution (Dako, Copenhagen, Denmark) for 10 min, followed by overnight incubation with an anti-CD31 antibody (1:50 dilution; Abcam, Cambridge, MA, USA) at 4 °C. After washing the slides, sections were treated with EnVision + HRP solution (Dako, Copenhagen, Denmark) for 1 h, and subsequently with Liquid DAB + Substrate mixture (Dako, Copenhagen, Denmark) for 8 min at room temperature, followed by brief hematoxylin counterstaining (1 s). After each step following antigen retrieval, all slides were washed in 1X wash buffer (Dako, Copenhagen, Denmark). CD31-positive area was quantified using Image J software under a light microscope at 10X and 20× magnification.

2.11. TUNEL assay for evaluating DNA damage in ovarian grafts

DNA fragmentation in ovarian grafts was assessed using the TUNEL assay on each observation day. After deparaffinization and rehydration, slides were treated with 0.8 % proteinase K (Dako, Copenhagen, Denmark) at room temperature for 20 min. Subsequently, they were incubated with a Cell Death Detection kit (Roche, Penzberg, Germany) at 37 °C for 1 h, followed by DPBS (WelGENE Inc., Korea) washing. The slides were mounted with VECTASHIELD (DAPI (4′,6-Diamidino-2-Phenylindole, dihydrochloride)-containing mounting solution; Vector Laboratories, Burlingame, CA, USA). TUNEL-positive cells emitted green fluorescence with excitation wavelengths of 450–500 nm and detection capabilities of 515–565 nm. Slides were examined under an inverted fluorescent microscope (Carl Zeiss AX10, Carl Zeiss AG, Oberkochen, Germany) at 10× magnification, and the TUNEL positive area was analyzed using AxioVision 4.8.2.0 software (Carl Zeiss MicroImaging, Oberkochen, Germany).

2.12. Superovulation, in vitro maturation (IVM), and in vitro fertilization (IVF) of retrieved oocytes from ovarian grafts, 21 days post-OTT

Twenty-one days post-OTT, each experimental group received intraperitoneal injections of 7.5 IU PMSG, followed by hCG injections (48 h later). Approximately 10 h after the hCG injection, ovarian grafts were retrieved in modified Medium-199 HEPES medium supplemented with 20 % FBS and 1 % PS. Antral follicles were punctured to collect cumulus-oocyte complexes (COCs), which were cultured in the same M − 199 medium with FSH and hCG for oocyte maturation. Matured oocytes were transferred to Human tubal fluid (HTF) medium, and the maturation rate was calculated as the number of metaphase II (MII) oocytes divided by the total retrieved oocytes. Concurrently, raw semen from 12-week-old B6D2F1 male mice was capacitated in HTF medium for 1 h. Ten μL of suspended sperm were added to oocytes. After 24 h, intact 2-cell stage embryos were counted, washed, and transferred to fresh KSOM medium. The fertilization rate was determined as the number of 2-cell stage embryos divided by the number of MII oocytes. The embryo development rate (blastocyst formation rate) was determined as the number of blastocysts divided by the number of 2-cell embryos after 72 h of culture. This procedure was replicated for four batches.

2.13. Reverse-transcription polymerase chain reaction (RT-PCR) and quantitative real-time PCR (qRT-PCR) in ovarian grafts retrieved 21 days post-OTT

Total RNA was extracted with TRIzol® reagent (Invitrogen, USA), followed by cDNA synthesis using random hexamers (Bioneer, Korea), dNTP (Mosaicon, Korea), Rnasin (Promega, Korea), and M-MLV reverse transcriptase (Promega, Korea). The resulting cDNA underwent 40 amplification cycles on the ViiA7 real-time PCR system (Applied Biosystems, USA) following the manufacturer's protocol. Fold changes were assessed using the $2^{-\triangle\triangle Ct}$ method, and log2 and Z-score transformed data were generated. Gene expressions for ovarian reserve-related genes (Fshr, Lhcgr, and Bax) and 84 angiogenesis-related genes were evaluated using specific primers obtained from Bioneer. Further details are provided in supplementary Data (Figs. S1 and S2).

2.14. Statistical analysis

Statistical analysis and graph preparation were carried out using GraphPad Prism version 10.0.0 software (California, San Diego). Each experiment involved a minimum of 10 animals, and the data presented represent the results obtained through more than three repetitions of both biological and technical experiments. For the evaluation of the number of follicles in the ovary, follicle quality, CD31 staining analysis, and TUNEL staining analysis, repeated measure two-way analysis of variances (ANOVA) and Tukey's multiple comparison tests were performed. In addition, ordinary one-way ANOVA and Tukey's comparisons test were conducted for the statistical consideration of in vitro and *ex vivo* analysis of angiogenic potential, IVF, PCR, and proteome profiling. All graphs were generated based on the mean ± standard deviation (SD), and the criteria for determining statistically significant differences were set as *p < 0.05, **p < 0.01, ***p < 0.001, and ****p < 0.0001. Each raw p-value is available in the following text or figure legends.

3. Results and discussion

3.1. Allogenic mouse L-PRP and H-PRP preparation and their derivatives' angiogenic potential assays (L-PFH(D), and H-PFH(D))

The platelet levels in allogeneic PRP were assessed and compared to whole blood (WB) in mice. The findings indicated a significant decrease of 0.004 ± 0.003-fold (****p < 0.0001) in PPP and a substantial increase of 5.487 ± 0.114-fold (****p < 0.0001) in PRP. This characterization aligns with the definition of PRP as a blood product containing 3 to 5 times more platelets than WB, confirming the suitability of our PRP for this study [50,51]. L-PRP was prepared by diluting H-PRP into PPP at a 1/4 ratio for subsequent experiments (Fig. 2 a, b). To assess the angiogenic potential of factors encapsulated in PFHs, both in vitro and *ex vivo* analyses were conducted using their derivatives (D) [52]. After 12 h of culture, the in vitro tube formation assay showed that L-PFH(D) exhibited the most intact and unbroken tubes compared to the control group. The number of branches in the in vitro tube formation assay for each group was as follows: Control, 34.750 ± 3.775; L-PFH(D), 61.000 ± 8.446; and H-PFH(D), 43.000 ± 10.950. Statistically significant results were observed, with high-quality blood vessel branches sprouting and extending in the L-PFH(D) group (Control vs. L-PFH(D), **p = 0.0039). Similar results were obtained on the 4th day of *ex vivo* culture (Control vs. L-PFH(D), *p = 0.0259) (Fig. 2 c). The number of branches in the *ex vivo* aortic ring assay for each group was as follows: Control, 1975.0 ± 711.2; L-PFH(D), 5890.0 ± 2351.0; and H-PFH(D), 845.0 ± 248.9. Interestingly, H-PFH(D), which contains a higher amount of pro-angiogenic factors, did not show a statistically significant difference from the control group, and its angiogenic potential was lower than that of L-PFH(D), both in vitro (L-PFH(D) vs. H-PFH(D), *p = 0.0322) and *ex vivo* (L-PFH(D) vs. H-PFH(D), *p = 0.0205) (Fig. 2 d). These findings suggest that the rapid initiation of angiogenesis due to an excessively high concentration of pro-angiogenic factors can lead to an imbalance in the essential factors required for the establishment of a robust vascular structure. This phenomenon is consistent with previous reports indicating that such an imbalance results in the excessive proliferation of unstable blood vessels, a common occurrence in cancer angiogenesis [53]. To delve deeper into this, we performed an extensive proteome array analysis to compare the composition and quantity of factors in the L-PFH and H-PFH preparations we generated.

3.2. The angiogenesis-related proteomes in PPP, L-PFH(D), and H-PFH (D)

In our analysis of angiogenesis-related factors, we compared L-PFH (D) with diluted platelets to H-PFH(D) with approximately fivefold concentrated platelets. Notably, five factors exhibited significant differences (Fig. 3 a, b): Angiopoietin-1 (Ang-1), Platelet-derived Growth Factor-AA and AB/BB (PDGF-AA and AB/BB), Plasminogen Activator Inhibitor-1 (PAI-1), and Platelet factor 4 (PF4) among others. Among pro-angiogenic factors, Ang-1 (*p = 0.0193), PDGF-AA (**p = 0.0043), and PlGF-2 (****p < 0.0001) were significantly higher in H-PFH(D) compared to L-PFH(D). HGF was exclusively detected in H-PFH(D) (****p < 0.0001), while OPN showed a significant decrease in H-PFH(D) compared to PPP and L-PFH(D) (PPP vs. H-PFH(D); **p = 0.0023, L-PFH (D) vs. H-PFH(D); **p = 0.0014). Additionally, MMP-9, crucial for

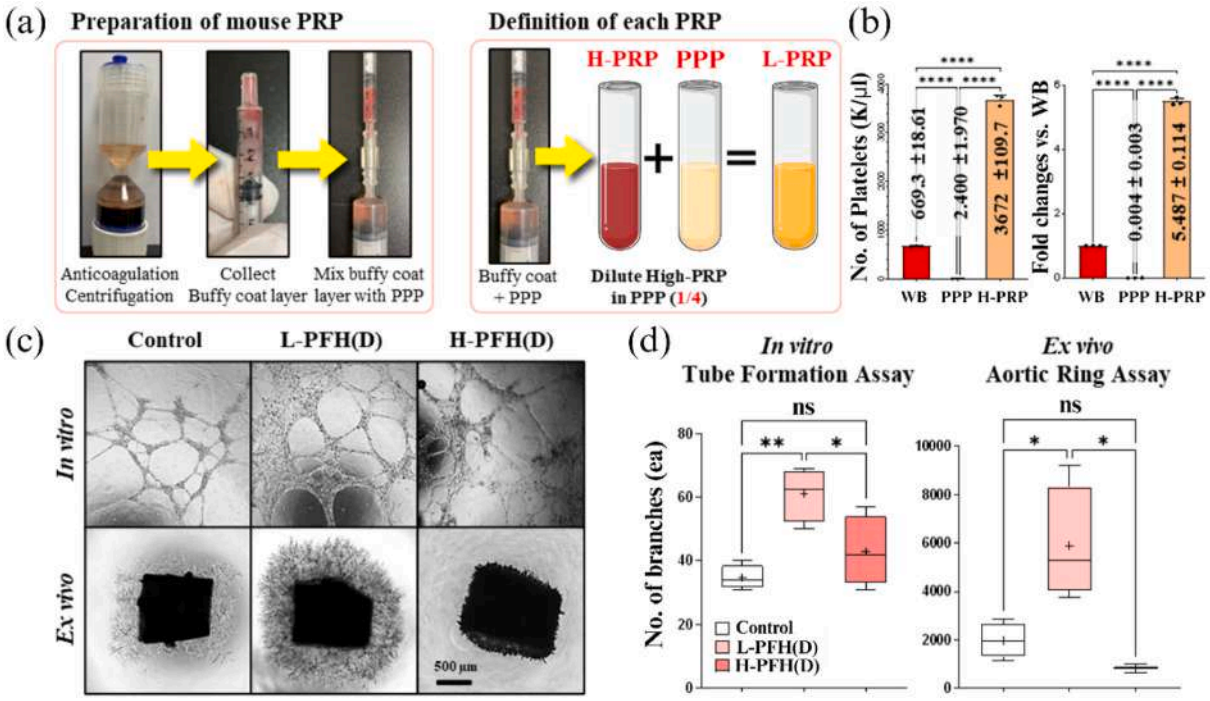

Fig. 2. Allogenic mouse L-PRP and H-PRP preparation and their derivatives' angiogenic potential assays (L-PFH(D), and H-PFH(D)). (a) Using a commercial PRP kit, H-PRP was prepared from allogeneic mouse blood, and L-PRP was generated by diluting H-PRP with PPP at a 1:4 ratio. (b) The platelet counts of whole blood, PPP, and PRP was assessed via C.B.C. test (n = 75, three replicates per PRP), ****$p < 0.0001$. (c) The figure shows in vitro (12 h post-seeding) and *ex vivo* (4 days post-seeding) angiogenic potential assays' microscopic images. (d) Graphs depict the branch numbers between HUVECs or sprouting from aortic segments.

initiating angiogenesis by degrading vessel basement membranes and surrounding ECMs, exhibited a significant decrease in H-PFH(D) compared to L-PFH(D) (L-PFH(D) vs. H-PFH(D); *$p = 0.0221$) (Fig. 3 c). Regarding anti-angiogenic factors, Endostatin showed no significant differences across groups. PF4 was not detected in H-PFH(D) but significantly increased in PPP compared to L-PFH(D) (L-PFH(D) vs. PPP; *$p = 0.0154$). Furthermore, TSP-2 and TIMP-1 were exclusively detected in PPP (TSP-2; ***$p = 0.0007$, TIMP-1; **$p = 0.0070$). TIMP-4 was not detected in L-PFH(D) but showed a significant increase in both PPP and H-PFH(D), with PPP exhibiting a significantly higher expression than H-PFH(D) (H-PFH(D) vs. PPP; **$p = 0.0041$) (Fig. 3 d). Factors related to angiogenesis initiation through hypoxia-induced inflammation signals and immune response also exhibited significant differences. CXCL-16 significantly decreased in PPP compared to L-PFH(D) (L-PFH(D) vs. PPP; *$p = 0.0475$), while CCL-2 was exclusively detected in PPP (****$p < 0.0001$). PTX-3 significantly increased in PPP compared to H-PFH(D) (H-PFH(D) vs. PPP; *$p = 0.0243$). PAI-1 was detected in both L- and H-PFH(D), with significantly higher expression in H-PFH(D) (L-PFH(D) vs. H-PFH(D); *$p = 0.0199$), and PEDF was significantly detected only in H-PFH(D) (*$p = 0.0248$) (Fig. 3 e). In summary, H-PFH exhibited predominantly higher levels of pro-angiogenic factors, while L-PFH, prepared by diluting platelets in relatively anti-angiogenic factor-rich platelet-poor plasma (PPP) with H-PRP, maintained a more balanced ratio of pro-angiogenic to anti-angiogenic factors compared to H-PFH (Fig. 3.). These findings suggest that anti-angiogenic factors may normalize dysfunctional vasculature, creating a favorable microenvironment for angiogenesis [54–57]. Additionally, anti-angiogenic factors can induce compensatory mechanisms, triggering pro-angiogenic factor release to restore blood supply [57–63]. Furthermore, anti-angiogenic factors can induce tissue hypoxia, initiating events that promote angiogenesis and restore oxygen supply to affected tissues. Moreover, anti-angiogenic factors can modulate immune responses and interact with immune cells, influencing angiogenesis and vascularization [28,54, 64–70]. In future experiments, we will explore potential pathological and molecular differences between L-PFH and H-PFH based on these findings. If significant indicators arise, they are expected to align with the discussions in this section.

3.3. Fabrication and characterization of FH-O, L-PFH, and H-PFH

To efficiently deliver PFs to the ovarian and subcutaneous microenvironments during transplantation, we meticulously compared and optimized the composition of Gel base (A) and Activator (B), referring to Yang et al. [45] (Fig. 4 a). The optimized composition included Gel base (A) with PRP, which underwent several trials to prevent premature gelation. By adjusting fibrinogen and aprotinin concentrations, we achieved a stable PRP-added Gel base (A) in a sol state. Gelation occurred only when exposed to Activator (B), aligning with our intentions. Upon adding Activator (B) composed of $CaCl_2$ and Thrombin to PRP-containing Gel base (A) and incubating for 30 min at room temperature, it completely polymerized into a gel state (Fig. 4 b). In rheological tests of FH-O, L-PFH, and H-PFH at body temperature, FH-O and L-PFH displayed similar storage and loss properties across all moduli. H-PFH exhibited greater physical rigidity compared to FH-O and L-PFH but there was no statistical significance (Fig. 4 c). Microstructural analysis of lyophilized hydrogels revealed that FH-O had a porous, thread-like structure due to low fibrinogen concentration. L-PFH displayed less porosity and a robust structure due to added platelets, while H-PFH exhibited a denser structure (Fig. 4 d). This difference can be attributed to the approximately fourfold higher platelet concentration in H-PFH, which enhances physical properties and reduces porosity [47]. Platelets play a role in entangling with fibrin clots and solidification [71–73] and the study confirmed that greater platelet numbers result in stronger physical properties and lower porosity. Studies indicate that the concentration and composition of PRP, platelet-rich fibrin (PRF), or platelet-rich blood clots can affect mechanical properties and in vivo outcomes [74–78]. After characterizing these materials, we successfully encapsulated mouse ovaries, ensuring complete coverage and maintenance of the outer ovarian surface (Fig. 4 e). Platelets, activated by contact with the extracellular matrix (ECM), aggregated, and tightly

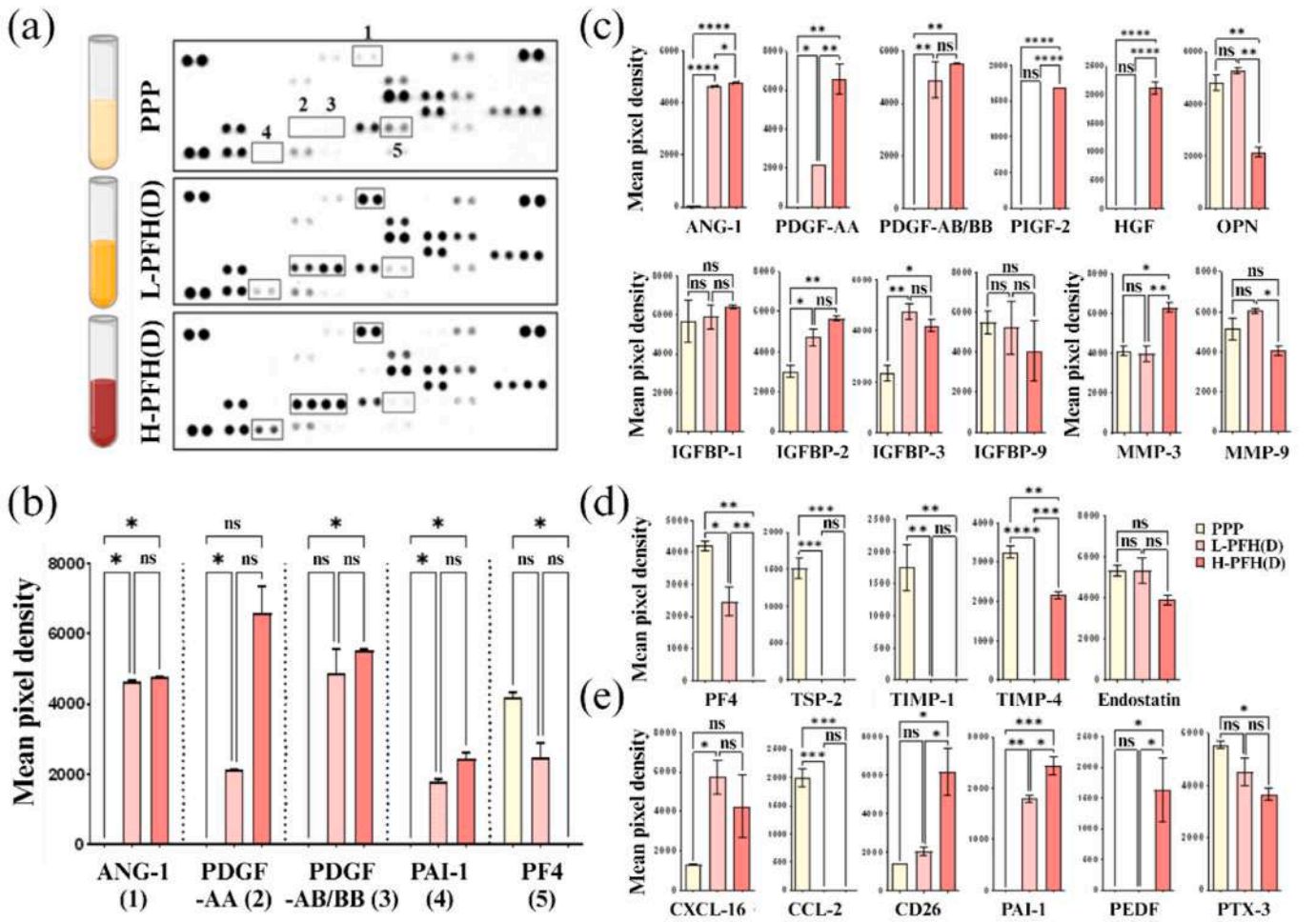

Fig. 3. The angiogenesis-related proteomes in PPP, L-PFH(D), and H-PFH(D). (a) Blotted membranes representing detected proteomes in each group. Boxes numbered from 1 to 5 highlight distinct blots. (b) Quantified data of top five divergent factors in each group. (c) Identified pro-angiogenic factors in PPP, L-PFH(D), and H-PFH(D). (d) Represented anti-angiogenic factors found in PPP, L-PFH(D), and H-PFH(D). (e) Inflammation-related pro- and anti-angiogenic factors detected in PPP, L-PFH(D), and H-PFH(D) (*p < 0.05, **p < 0.01, ***p < 0.001, and ****p < 0.0001).

adhered, ensuring the hydrogel layer's stability after encapsulation [46].

Furthermore, we explored an injectable PFH formulation using a dual syringe tip. By connecting PRP-containing Gel base (A) to the left syringe and Activator (B) to the right syringe, we achieved gel formation upon simultaneous injection (Fig. S3). This versatile approach demonstrates PFH's adaptability, extending not only to physical properties and shapes but also to application methods [79]. This adaptability opens avenues for diverse therapeutic interventions in tissue engineering, regenerative medicine, and beyond. Continued investigation and optimization of the injectable PFH formulation hold promise for broader clinical applications, not only in personalized FP therapy but also in other medical fields [80].

3.4. The vessel formation on each observation day and ovarian response against the gonadotropin

We transplanted encapsulated ovaries subcutaneously into the dorsal region of mice, selecting this site due to reported severe ischemic damage during ovarian transplantation, which allows for clear graft observation in challenging conditions [13]. Macroscopic evaluations were conducted at 1-, 3-, 7-, and 21-days post-transplantation to assess graft condition, size, color, and surrounding blood vessels. These observations tracked graft viability and physiological changes over time before tissue collection. Angiogenesis after avascular ovarian transplantation involves multiple stages and can vary due to individual health and surgical techniques [17,81]. In the initial 24 h post-transplantation, grafts rely on oxygen and nutrient diffusion, supporting cells near the graft surface. Our results showed no significant changes in the sham group, but experimental groups displayed extended vascular structures surrounding the encapsulated ovaries. L-PFH and H-PFH exhibited higher vessel abundance compared to FH-O, with thicker and more numerous vessels (Fig. 5 a), indicating that platelets and their factors expedite angiogenesis around the encapsulated ovaries. It is known that inflammatory responses initiated 24–48 h post-transplantation release various cytokines and chemokines, aiding in angiogenesis cell recruitment [62,64,82]. Plus, by days 2–5, endothelial cells begin forming rudimentary vascular networks, guided by pro-angiogenic factors from hypoxic graft cells and immune cells that received inflammatory signals [60,65,66,83]. On day 3, evidence of blood vessels was observed, though they were not fully stabilized, leading to bleeding consistent with angiogenesis. Interestingly, the sham group exhibited less bleeding than the other groups. H-PFH displayed a hardened graft with black liquid, indicating substantial bleeding or coagulated blood. Conversely, FH-O and L-PFH groups exhibited similar bleeding levels (Fig. 5 a). From day 4 to a week post-transplantation, primitive vascular networks mature into functioning blood vessels, recruiting pericytes and smooth muscle cells to stabilize them [54, 58–62]. By weeks 2–3, the newly formed vessels should supply adequate blood flow, restoring function [54,58–62]. The absence of hematoxylin

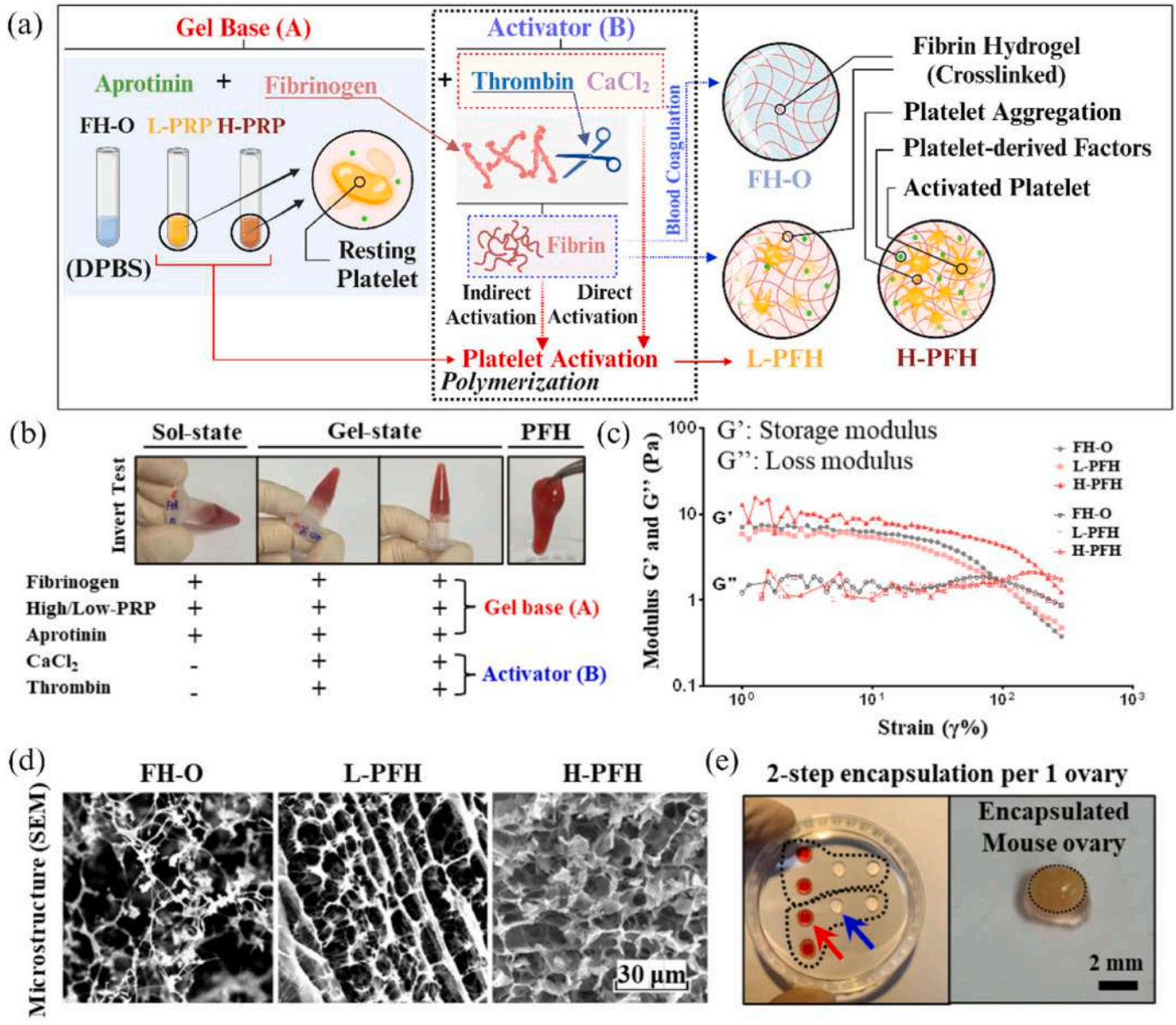

Fig. 4. Fabrication and characterization of FH-O, L-PFH, and H-PFH. (a) Schematic illustration of L-PFH and H-PFH fabrication procedure (Created with BioRender.com). (b) Test tube inversion assay of PFH post Gel base (A) and Activator (B) mix. (c) Mechanical properties of each hydrogel. Both storage modulus (G′) and loss modulus (G″) showed higher values in H-PFH compared to FH-O and L-PFH. (d) Microstructure of each hydrogel. Porosity density increased in a platelet concentration-dependent manner. (e) Procedure of ovary encapsulation and resultant encapsulated ovary (Red arrow points to Gel base (A) with PRP, blue arrow to Activator (B)).

staining and the presence of only a pale pink color in the locations where nuclei should be observed in histological analysis could be attributed to fibrosis or necrosis [84]. Additionally, as evident from TUNEL staining, a positive signal was observed in the same area, indicating damage to the nuclei due to necrotic death [85]. Day 7 showed the Sham group with necrotic death due to unsuccessful engraftment. In contrast, L-PFH exhibited robust blood vessels near the ovary, resembling normal ovaries, while H-PFH showed some surrounding blood vessels with bleeding. Day 21 revealed clear graft-recipient-connected vessels in L-PFH and H-PFH. However, H-PFH exhibited high-permeability vessels, indicative of excessive angiogenesis, potentially due to the higher concentration of proangiogenic factors, leading to imbalanced angiogenesis. Although we did not quantitatively or directly assess vessel permeability, we confirmed indirectly through literatures that the observation of hemorrhage around the tissue after avacular transplantation during visual inspection serves as an indirect explanation for the increased vessel permeability [86]. Furthermore, it is well known that hemorrhage from a increased vessel permeability often accompanies the initiation stages of neovascularization and angiogenesis in tumors or in the neovascularization process related to retinal disease [87]. This can compromise vessel integrity and functionality, underscoring the need for a balanced proangiogenic factor concentration to ensure proper angiogenesis, creating functional, non-leaky blood vessels in transplanted ovaries (Fig. 5 a).

To evaluate ovarian functional recovery, rapid follicle growth and hormonal response were key indicators (Fig. 5 a). PMSG, acting like FSH, was injected into normal mice and two mice from each experimental group 48 h before the 21st day. The results showed a significant weight decrease in all groups on day 3 compared to the Fresh group (Sham; 2.275 ± 0.714 mg, ***p = 0.0009, FH-O; 2.400 ± 0.583 mg, **p = 0.0012, L-PFH; 2.525 ± 1.124 mg, **p = 0.0015, and H-PFH; 3.375 ± 1.823 mg, **p = 0.0075). On day 7, the Sham and FH-O groups

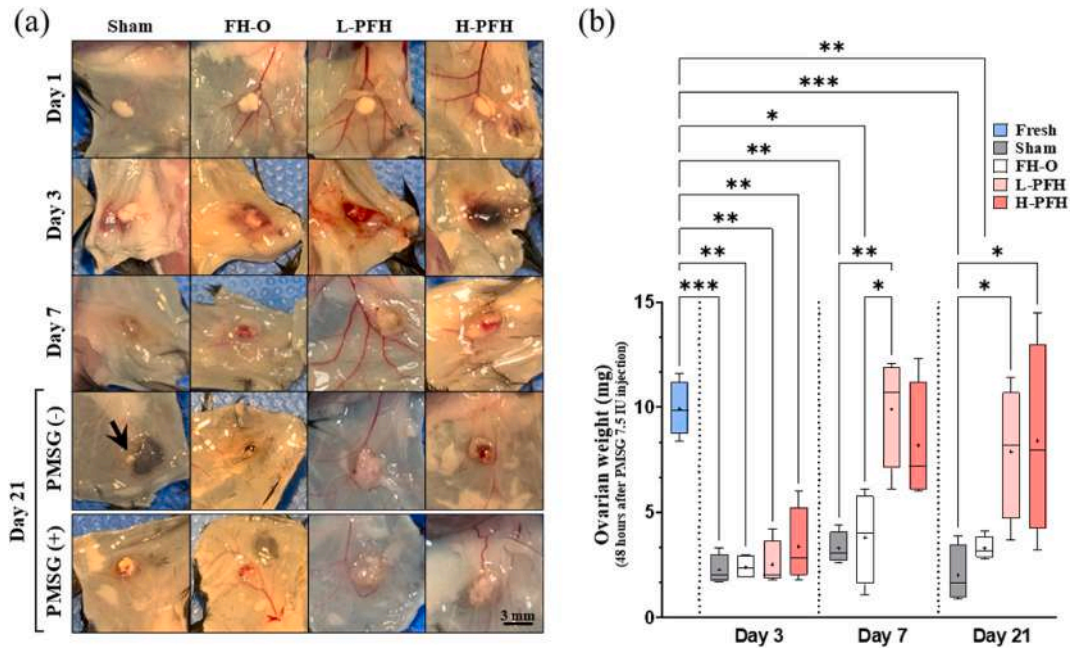

Fig. 5. The vessel formation on each observation day and ovarian response against the gonadotropin. (a) Visualization of vessel formation around the graft at intervals of 1-, 3-, 7-, and 21 days post-transplantation. (b) Comparison of ovarian weights in each group (n = 4/group) at days 3, 7, and 21 post-transplantations, following PMSG administration 48 h prior to sampling. The PFH groups presented comparable weights to the fresh ovary from PMSG-treated mice on days 7 and 21. (*p < 0.05, **p < 0.01, and ***p < 0.001).

exhibited significantly lower weights than the Fresh group. Conversely, L-PFH and H-PFH groups showed no significant differences. On day 21, L-PFH and H-PFH groups exhibited no significant differences compared to the Fresh group, indicating functional recovery like normal ovaries. However, the Sham and FH-O groups displayed significantly decreased weights compared to the Fresh group. The Sham group also exhibited significantly lower weight than L-PFH and H-PFH groups (Fig. 5 b).

These results suggest that PRP facilitates rapid and stable blood vessel formation. Differences between L-PFH and H-PFH indicate variations in L- and H-PRP derivatives, contributing to distinct effects. Platelet numbers and activation status influence factor secretion, and interactions between these factors vary. Notably, pro-angiogenic and anti-angiogenic factors play a crucial role, and their balance differs depending on the specific tissue or microenvironment [47,56,58,88].

Our findings suggest that L-PFH is more effective in promoting intact vessel formation and endocrine function recovery in transplanted ovaries, emphasizing the importance of L-PFH's specific composition and properties, including factors secreted by activated platelets, in supporting functional blood vessel formation and hormonal restoration in the grafts.

3.5. Recovery of ovarian reserve: the quantity and quality of remaining follicles and ovarian reserve-related gene expressions

Through pathological evaluation of ovarian tissues collected on various post-transplantation days, significant findings emerged. On day 1 post-transplantation, signs of ongoing follicular degeneration, specifically atresia in the remaining growing follicles, were observed. The total number of follicles and the ratio of G1 follicles to total follicles exhibited no significant differences among the groups. However, starting from the 3rd day after transplantation, an increase in the eosinophilic area in the stromal region, indicative of ischemic necrosis, was visually observed in the Sham, FH-O, and H-PFH groups but not in the L-PFH group (Fig. 6 a). Additionally, the total number of follicles remaining in the ovary significantly differed, with L-PFH (126.200 ± 24.809) showing a significantly higher number compared to all other groups (Sham; 75.400 ± 10.840, ***p = 0.0003, FH-O; 69.400 ± 18.110, ***p = 0.0001, and H-PFH; 94.900 ± 15.423, *p = 0.0189) (Fig. 6 c). On the 7th day post-transplantation, significant differences were noted upon pathological examination. In particular, the morphology of the L-PFH group closely resembled that of fresh ovaries, indicating a healthier state with primordial follicle nests around the cortex region of the grafts (Fig. 6 a, b). The total number of follicles was highest in L-PFH (114.300 ± 37.606), followed by H-PFH (83.500 ± 16.099), FH-O (62.600 ± 23.156), and Sham (33.800 ± 8.053). The proportion of preserved follicles was also highest in L-PFH (74.760 ± 7.130 %), followed by H-PFH (69.310 ± 7.696 %), FH-O (40.830 ± 16.909 %), and Sham (23.090 ± 7.702 %). Significant differences were observed between L-PFH and Sham (***p = 0.0003) and FH-O (**p = 0.0097). There was no significant difference between FH-O and H-PFH. Similar trends were observed on day 21, with L-PFH exhibiting significantly higher follicle quantity (*p = 0.0351) and follicle quality (***p = 0.0003) compared to H-PFH. However, there was no significant difference in follicle quantity (ns, p = 0.2840) and quality (ns, p = 0.0541) between FH-O and H-PFH (Fig. 6 d). The proportion of each follicle according to their developmental stages was similar among all groups, but when considering this in conjunction with the total number of preserved follicles in each group, L-PFH demonstrated a protective effect in preserving the primordial follicle pools, which represent the ovarian reserve (Fig. S4).

In summary, L-PFH proved superior in preserving both follicle quantity and quality (Fig. 6 b-d). FH-O and H-PFH also exhibited better follicle preservation and improved quality compared to the Sham group. Notably, there was no significant difference between FH-O and H-PFH. L-PFH's composition, a mixture of PPP and H-PRP, likely contributes to its enhanced performance. As observed in proteome screening results, the distribution of proangiogenic and anti-angiogenic factors in L-PFH is more balanced compared to H-PFH. This suggests that while H-PFH promotes rapid angiogenesis initiation, L-PFH fosters the formation of stable blood vessels due to its higher concentration of anti-angiogenic factors. These findings align with prior studies emphasizing the importance of pro-angiogenic and anti-angiogenic factor interaction and balance in achieving intact and functional blood vessel formation [56,58,88]. Moreover, the quicker angiogenesis initiation in PRP-based groups

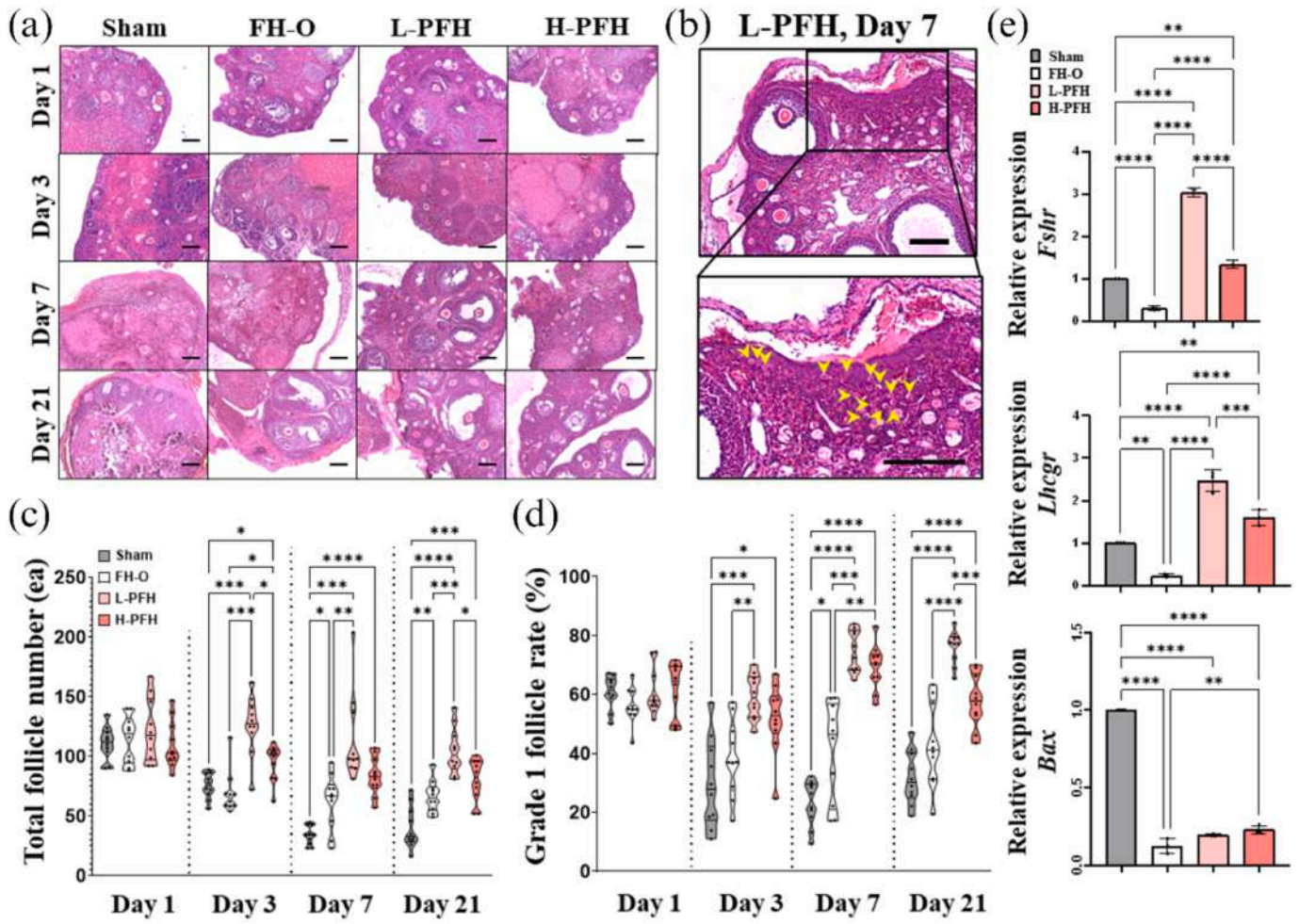

Fig. 6. Recovery of ovarian reserve: The quantity and quality of remaining follicles and ovarian reserve-related gene expressions. (a) Histological evaluation of graft samples, visualized with H&E staining. Each scale bar denotes 100 μm. (b) On Day 7, L-PFH group demonstrated primordial follicle nests, a significant indicator of healthy ovarian reserve (highlighted by yellow arrowheads). (c) The total follicle count per group with proportionate representation of follicular developmental stages provided in Fig. S2. (d) Comparison of high-quality follicles (G1) to the overall follicle count across groups (n = 10/group). (e) Expressions of ovarian reserve markers (Fshr, Lhcgr), and DNA fragmentation marker (Bax) were confirmed via quantitative real-time PCR (qRT-PCR).

compared to Sham and FH-O groups can be attributed to the presence of immune cells and pre-existing angiogenic factors in PRP, expediting the response to tissue hypoxia and transplantation-related injuries [55,64]. Notably, complete tissue engraftment and functional blood vessel establishment usually require around three weeks [24]. Accordingly, gene expression assessment on day 21 revealed consistent trends. Fshr and Lhcgr expression, representative markers of ovarian function, were significantly higher in L-PFH compared to all other groups, while it was significantly lower in Sham [45]. Fshr expression in H-PFH was significantly lower compared to L-PFH, with no significant difference in Bax expression between L-PFH and H-PFH. Interestingly, cell death was significantly reduced in all groups compared to Sham, and FH-O exhibited a significantly stronger anti-apoptotic effect than H-PFH (Fig. 6 e). These findings suggest that a moderate concentration of platelet-derived factors, as seen in FH-O or when applying fibrin alone, can effectively prevent apoptosis.

3.6. Vascular endothelial cells and DNA fragmentation in ovarian grafts

To evaluate post-transplantation changes in blood vessel formation and cell death within ovarian tissue, we performed CD31 staining to visualize blood vessel structures and TUNEL staining to detect DNA fragmentation. No significant differences in blood vessel quantity or apoptosis were observed among the groups on the first day after transplantation (Fig. 7 a, b). However, from the third day onward, while blood vessel quantity remained similar, DNA fragmentation significantly decreased in L-PFH (***p = 0.0007) and H-PFH (**p = 0.0051) compared to the Sham group. FH-O did not show significant differences compared to any of the groups (Fig. 7 d, f). By the 7th day post-transplantation, the CD31-positive area, indicative of blood vessel presence, significantly increased in L-PFH compared to Sham (*p = 0.0296) and FH-O (*p = 0.0193), consistent with H&E staining results (Fig. 7 a-c). There were no significant differences in blood vessel quantity among the PFH groups. DNA fragmentation analysis revealed a significant decrease in the ratio of positive areas in all groups compared to Sham on day 7 (FH–O; *p = 0.0432, L-PFH; *p = 0.0238, and H-PFH; *p = 0.0396). However, there were no significant differences in DNA fragmentation between FH-O, L-PFH, and H-PFH (Fig. 7 d-f).

On day 21, the vascular ratio remained significantly higher in L-PFH compared to Sham (*p = 0.0113) and FH-O (*p = 0.0185), consistent with the observations on day 7. There were no significant differences in the vascular ratio in H-PFH compared to all groups (Fig. 7 c). No significant differences were found in the quantified data of DNA fragmentation among the groups on day 21, indicating a comparable level of cell death in all groups at that time point (Fig. 7 f). In summary, our results support previous findings, demonstrating that L-PFH promotes faster and more complete blood vessel formation, ultimately improving tissue survival. Ischemic necrosis is a prominent feature observed in

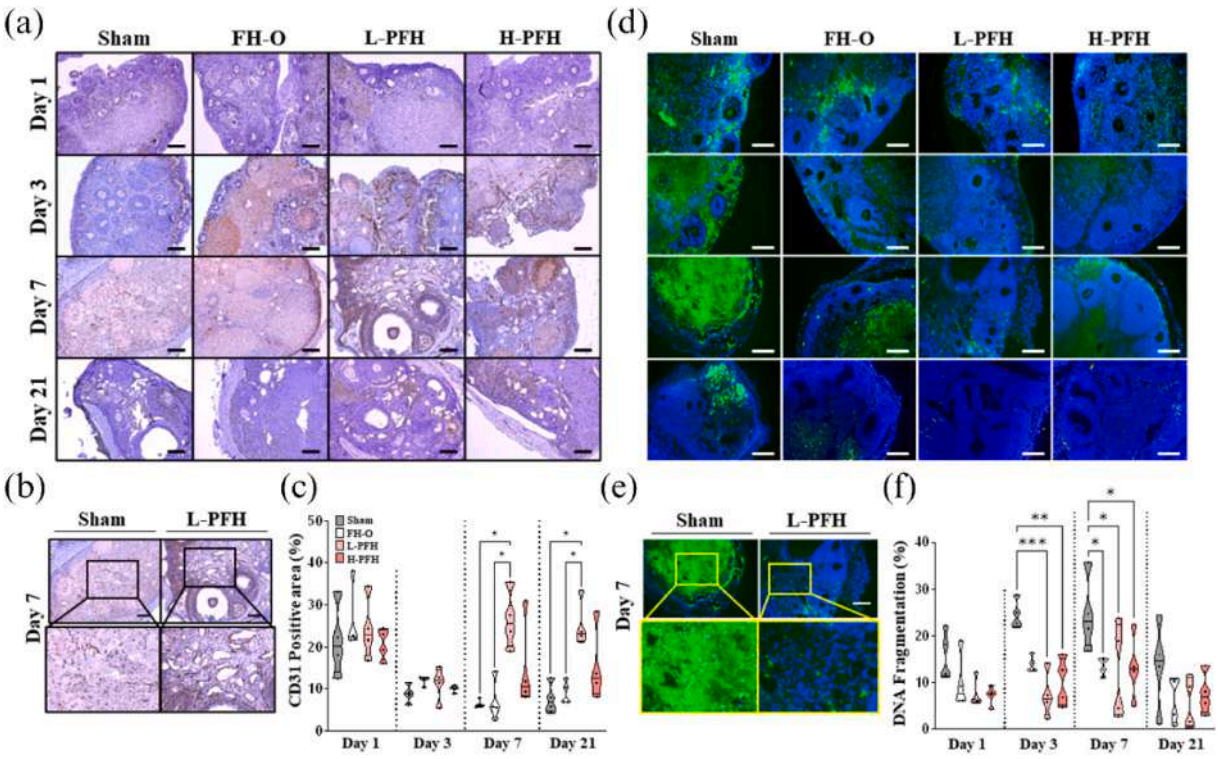

Fig. 7. Vascular endothelial cells and DNA fragmentation in ovarian grafts. (a) Microscopic views of CD31-Immunohistochemistry: Hematoxylin counterstain depicts nuclei in blue and DAB + signifies CD31 positive vascular endothelial cells in brown. (b) On Day 7, the L-PFH exhibited elevated levels of CD31, resembling a healthy, fresh ovary. Conversely, the Sham and FH-O displayed sparse nuclei, suggestive of stromal damage from ischemic necrosis, with ghosted cells appearing in the stromal regions. (c) Quantification of CD31 positive ratios across the groups. (d) DNA fragmentation visualized using TUNEL assay: FITC highlights DNA fragmentation in green, and DAPI depicts nuclei in blue. (e) Seven days post-transplantation, the PFH-treated groups showed notably reduced DNA damage. Conversely, the Sham group demonstrated severe DNA damage and nuclear loss in comparison to the L-PFH group at the same time point. (f) Quantified data of TUNEL positive areas across each group. (*p < 0.05, **p < 0.01, ***p < 0.001).

tissues subjected to ischemic injury, with DNA fragmentation serving as a reliable indicator of this process [89]. Our results show a correlation between reduced vessel density and increased DNA fragmentation, while well-maintained or increased vessel density resulted in minimal DNA injury. This suggests that PFH-treated groups, in general, exhibited accelerated blood vessel formation, thereby mitigating tissue ischemic damage, and reducing DNA injury. Notably, L-PFH exhibited superior efficacy in preventing such damage, highlighting its potential as a robust protective agent.

3.7. Angiogenesis-related gene expressions in ovarian grafts

Gene expression analysis at 21 days post-transplantation compared to healthy ovaries. PFH-treated groups resembled the Fresh group, with H-PFH expressing more factors than L-PFH. The angiogenesis-related gene expressions were increased in all experimental groups compared to the Fresh group, however, the L-PFH showed similar expression patterns with the Fresh group with no significance. This result projects the effect of difference balance between pro- and anti-angiogenic factors detected in each hydrogel (Fig. 3). FH-O had the highest gene over-expression, while Sham under-expressed most genes (Fig. 8 a). Genes responding to hypoxic shock (*Akt1*, *Egf*, *Epas*, *Hifα*, *Tgfα*, *Vegfa*, *Vegfb*, *Vegfc*, *Fgf1*, and *Fgf2)* and inflammation (*Ccl2*, *Ccl1*, *Il-1β*, *Il-6*, and *TNFα)* showed similar patterns in L-PFH compared to normal ovarian gene expression, with no significant difference (Fig. 8 b-c). Overall, genes decreased in the Sham group compared to normal ovaries (Fig. 8 a-c). These findings highlight the importance of achieving a well-balanced equilibrium between pro-angiogenic and anti-angiogenic factors for successful neovascularization (Fig. 8 d). A balance between pro- and anti-angiogenic factors is crucial for efficient neovascularization [53]. Excessive pro-angiogenic signaling can lead to aggressive, leaky blood vessels, promoting metastasis [90]. Maintaining balance encourages healthy vessel formation, minimizing tissue damage during engraftment [91–94]. These results align with established literature theories, suggesting tissues may signal for blood vessel formation when FH-O and H-PFH have excessive gene expression (Fig. 8 d) [53–64]. The L-PFH group showed better outcomes in all assessment indexes in this study, which could be explained by these reasons. Conversely, the severely diminished gene expression in the Sham group suggests early-stage tissue damage and total functional loss. Considerations include ovarian dynamic changes during the estrous cycle and ovulation, a comprehensive gene expression pattern analysis from the initial to the 21st day would offer a more accurate understanding.

3.8. Recovery of ovarian function: production of healthy and fertile oocytes

On the 21st day post-OTT, we induced superovulation in each experimental group and retrieved ovarian grafts before ovulation to recover oocytes from growing follicles. We conducted a total of four independent experiments, and the combined results of these replicates are presented in Table 1. The number of oocytes obtained from each group, based on 18 mice per group, were as follows: Sham (39), FH-O (58), L-PFH (202), and H-PFH (128). Remarkably, the L-PFH group exhibited a significantly higher number of oocytes compared to the Sham group (*p = 0.0440), and a significant increase in the number of oocytes recovered per individual on average was observed in the L-PFH group compared to the Sham (*p = 0.0128) and FH-O (*p = 0.0241). Although not statistically significant, there was a tendency for an increased number of MII oocytes (Sham: 6, FH-O: 19, L-PFH: 50, and H-

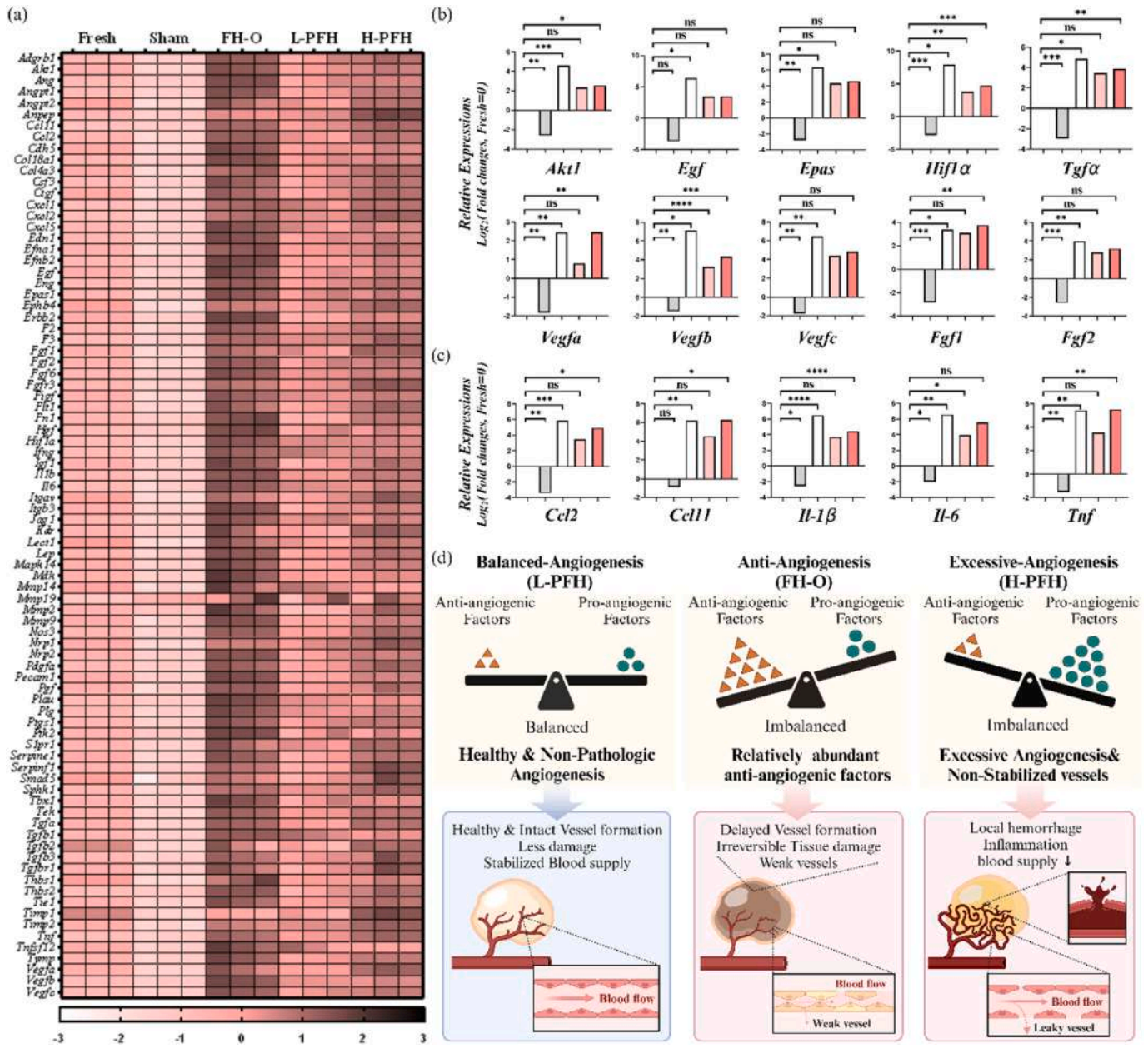

Fig. 8. Angiogenesis-related gene expressions in ovarian grafts. (a) Heatmap depicting expression patterns of angiogenesis-related genes across various groups, facilitating extensive intergroup comparisons. The full name of genes is available in Table S3. (b) Analysis of gene expression changes in the ovary on the 21st day after transplantation, comparing Log2 transformed fold-change values among all groups, revealed the upregulation of vascular-related factors in response to hypoxic shock exposure. Detailed data can be found in Fig. S5 (Fresh = 0 in all graphs, gray: Sham, white: FH-O, pink: L-PFH, and red: H-PFH). (c) Analysis of gene expression changes in the ovary on the 21st day after transplantation, comparing Log2 transformed fold-change values among all groups, revealed the upregulation of vascular-related factors in response to inflammatory signals. Detailed data can be found in Fig. S5, (Fresh = 0 in all graphs, gray: Sham, white: FH-O, pink: L-PFH, and red: H-PFH). (d) Schematic summary of the study. The balance of factors surrounding ovarian tissues immediately post-avascular transplantation is vital for the formation of intact, functional vessels (Created with BioRender.com), which determines the organ's survival and functions. (ns: no significance, *p < 0.05, **p < 0.01, ***p < 0.001 and ****p < 0.0001).

Table 1
The result of superovulation, in vitro maturation, and fertilization.

Groups	No. of mouse	No. of oocyte	Mean No. of oocyte	No. of MII	MII (%)	No. of 2-cell	2-cell (%)	No. of blastocyst	Blastocyst (%)
Sham	18	39	2.2	6	15.4 %	2	33.3 %	1	50.0 %
FH-O	18	58	3.2	19	32.8 %	11	57.9 %	4	36.4 %
L-PFH	18	202	11.2	50	24.8 %	31	62.0 %	21	67.7 %
H-PFH	18	128	7.1	32	25.0 %	19	59.4 %	6	31.6 %

The number of oocytes retrieved from each group (n = 18/group) and blastocyst formation rates were significantly higher in the L-PFH group (*p < 0.05). This table exhibits the total result of 4 replicated batches (Table S2).

PFH: 32) and a higher maturation rate (Sham: 15.4 %, FH-O: 32.8 %, L-PFH: 24.8 %, and H-PFH: 25.0 %) in all experimental groups compared to the Sham group (Fig. 9 a, b). Regarding the number of 2-cell stage embryos (Sham: 2, FH-O: 11, L-PFH: 31, and H-PFH: 19) and the fertilization rate (Sham: 33.3 %, FH-O: 57.9 %, L-PFH: 62.0 %, and H-PFH: 59.4 %), there was a general trend of higher values in the PFH treatment groups compared to the Sham and FH-O groups, with L-PFH exhibiting the highest tendency. However, these differences did not reach statistical significance. Notably, the percentage of fertilized embryos that successfully developed into blastocysts (Sham: 50.0 %, FH-O: 36.4 %, L-PFH: 67.7 %, and H-PFH: 31.6 %) was significantly higher in the L-PFH group compared to the FH-O group (*p = 0.0419) (Fig. 9, Table 1 and Table S2).

Our findings indicate that L-PFH exhibited superior outcomes, with a higher number of retrieved oocytes and a greater proportion of healthy embryo development into blastocysts. This suggests that platelet-derived factors encapsulated in L-PFH provide optimal conditions for preserving ovarian follicles. In contrast, despite containing relatively higher levels of angiogenesis-promoting factors, the H-PFH group showed poorer results due to the formation of excessive and unhealthy blood vessels. Our data reveals that the presence of a relatively high concentration of angiogenesis-promoting factors against anti-angiogenic factors does not guarantee the formation of robust blood vessels. Instead, a delicate balance between pro-angiogenic factors, anti-

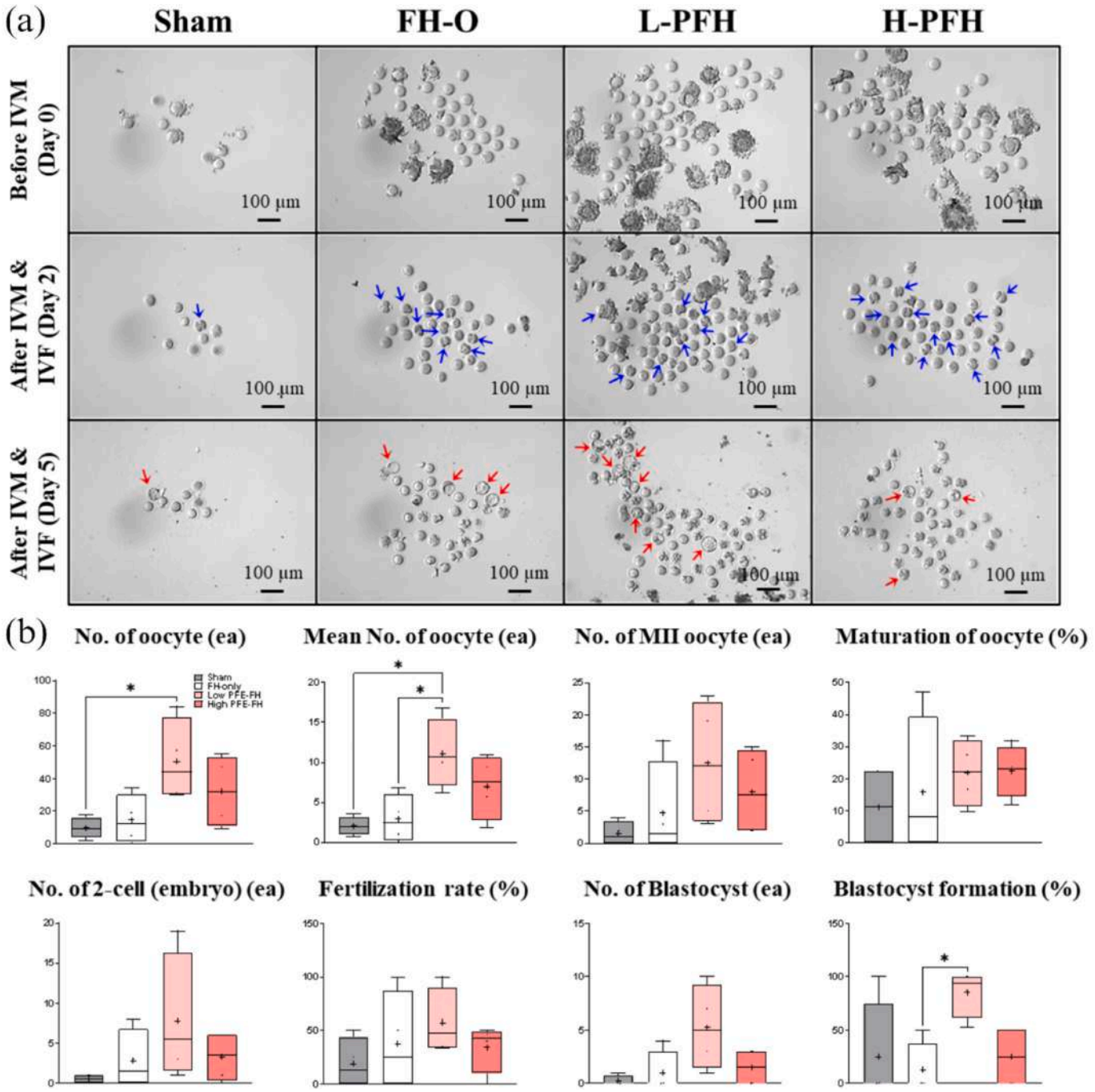

Fig. 9. Recovery of ovarian function: production of healthy and fertile oocytes. (a) The representative images of this experiment (batch 3 from Table S2). The blue arrow indicates 2-cell stage embryos, and the red arrow indicates blastocysts. (b) The number of retrieved oocytes and successful embryo development into healthy blastocysts were significantly higher in the L-PFH. (*p < 0.05).

angiogenic factors, and mediators of the inflammatory response is crucial. The L-PFH treatment created an environment conducive to tissue grafting, ensuring tissue survival, follicle preservation, and other favorable outcomes. Our comprehensive analysis of proteome, histology, gene expression, and other results leads us to conclude that the key to preventing tissue damage during avascular transplantation lies in the rapid establishment and connection of healthy and functional blood vessels, achieved by supplying the optimal balance of angiogenesis-related factors. However, the precise composition ratio required for achieving this "functional vessel formation" may vary depending on the anatomical location, organ type, and microenvironment involved.

4. Conclusion

We have successfully developed a hydrogel utilizing autologous blood to mimic the blood coagulation process, thereby facilitating avascular ovarian tissue transplantation (OTT). Our study has yielded remarkable outcomes with the use of the L-PFH compared to the H-PFH. We observed significant enhancements in follicle survival, accelerated vascularization, improved tissue viability, preservation of primordial follicles, elevated endothelial cell expression, and prevention of ischemia-induced necrosis in the stromal region. Our research underscores the critical significance of maintaining a balanced composition of pro-angiogenic and anti-angiogenic factors for successful neovascularization, a characteristic notably prominent in L-PFH. Furthermore, the customizable properties of this hydrogel make it conducive to potential personalized regenerative therapies, offering safe and cost-effective vascularization treatments.

These results highlight the paramount importance of efficient and prompt neovascularization in OTT, especially in ischemic microenvironments for fertility preservation. The encapsulation of platelet-derived factors in the hydrogel confers several benefits, including nutrient supply, ischemic protection, and improved follicle survival. Local administration of platelet-derived factors also expedites revascularization and enhances immune responses. It is essential to acknowledge the limitations of our study, primarily relying on rodent models, which may introduce biases and hinder the direct translation of our findings to human applications. The utilization of allogeneic PRP introduces an element of variability that could potentially affect our results, compounded by the lack of standardized protocols for PRP production, which further complicates consistency and reproducibility.

In summary, our research demonstrates that localized delivery of platelet-derived factors through a fibrin scaffold offers numerous advantages, promoting angiogenesis in ovarian tissues. Our findings have the potential to revolutionize not only fertility preservation but also areas requiring localized blood vessel formation and personalized regenerative medicine, offering a safe and cost-effective solution.

CRediT authorship contribution statement

Nanum Chung: Writing – original draft, Visualization, Validation, Software, Methodology, Investigation, Formal analysis, Data curation, Conceptualization. **Chungmo Yang:** Writing – review & editing, Validation, Methodology, Data curation, Conceptualization. **Heeseon Yang:** Writing – review & editing, Writing – original draft, Visualization, Investigation, Data curation. **Jungwoo Shin:** Writing – review & editing, Investigation. **Chae Young Song:** Writing – review & editing, Methodology, Investigation. **Hyewon Min:** Writing – review & editing, Visualization. **Ji Hyang Kim:** Writing – review & editing, Supervision, Resources, Funding acquisition. **Kangwon Lee:** Writing – review & editing, Supervision, Resources, Project administration, Funding acquisition. **Jung Ryeol Lee:** Writing – review & editing, Supervision, Resources, Project administration, Funding acquisition.

Declaration of competing interest

The authors declare that they have no known competing financial interests or personal relationships that could have appeared to influence the work reported in this paper.

Data availability

Data will be made available on request.

Acknowledgments

This work was supported by the grant of the Korea Health Technology R&D Project through the Korea Health Industry Development Institute (KHIDI), funded by the Ministry of Health & Welfare, Republic of Korea (grant number: HI22C1394 to J.R.L), supported by the National Research Foundation of Korea (NRF) grant funded by the Korea government (MSIT) (grant number: 2021R1C1C1004418 to J.H.K.) and supported by the grant from theSeoul National University Bundang Hospital (SNUBH) Research Fund (grant number: 13-2020-016 to J.R.L).

Appendix A. Supplementary data

Supplementary data to this article can be found online at https://doi.org/10.1016/j.biomaterials.2024.122768.

References

[1] J. Donnez, M.-M. Dolmans, Fertility preservation in women, N. Engl. J. Med. 377 (2017) 1657–1665, https://doi.org/10.1056/nejmra1614676.
[2] J. Donnez, M.-M. Dolmans, Fertility preservation in women, Nat. Rev. Endocrinol. 9 (2013) 735–749, https://doi.org/10.1038/nrendo.2013.205.
[3] M. De Vos, J. Smitz, T.K. Woodruff, Fertility preservation in women with cancer, Lancet 384 (2014) 1302–1310, https://doi.org/10.1016/S0140-6736(14)60834-5.
[4] M.E. Gornet, L.X. Chen, M.S. Christianson, Ovarian tissue cryopreservation for emerging primary ovarian insufficiency: expanding indications outside of cancer to preserve fertility and increase access to care, Fertil. Steril. 118 (2022) 985–986, https://doi.org/10.1016/j.fertnstert.2022.09.002.
[5] N. Resetkova, M. Hayashi, L.A. Kolp, M.S. Christianson, Fertility preservation for prepubertal girls: update and current challenges, Curr Obstet Gynecol Rep 2 (2013) 218–225, https://doi.org/10.1007/s13669-013-0060-9.
[6] E.J. Hoekman, L.A. Louwe, M. Rooijers, L.A.J. Westerlaken, N.F. Klijn, G.S. K. Pilgram, C.D. Kroon, C.G.J.M. Hilders, Ovarian tissue cryopreservation: low usage rates and high live-birth rate after transplantation, Acta Obstet. Gynecol. Scand. 99 (2020) 213–221, https://doi.org/10.1111/aogs.13735.
[7] H.S. Kong, E.J. Kim, H.W. Youm, S.K. Kim, J.R. Lee, C.S. Suh, S.H. Kim, Improvement in ovarian tissue quality with supplementation of antifreeze protein during warming of vitrified mouse ovarian tissue, Yonsei Med. J. 59 (2018), https://doi.org/10.3349/ymj.2018.59.2.331.
[8] M.K. Kim, H.S. Kong, H.W. Youm, B.C. Jee, Effects of supplementation with antifreeze proteins on the follicular integrity of vitrified-warmed mouse ovaries: comparison of two types of antifreeze proteins alone and in combination, Clin Exp Reprod Med. 44 (2017), https://doi.org/10.5653/cerm.2017.44.1.8.
[9] J.R. Lee, H.W. Youm, H.J. Lee, B.C. Jee, C.S. Suh, S.H. Kim, Effect of antifreeze protein on mouse ovarian tissue cryopreservation and transplantation, Yonsei Med. J. 56 (2015), https://doi.org/10.3349/ymj.2015.56.3.778.
[10] J. Lee, J.R. Lee, H.W. Youm, C.S. Suh, S.H. Kim, Effect of preoperative simvastatin treatment on transplantation of cryopreserved-warmed mouse ovarian tissue quality, Theriogenology 83 (2015), https://doi.org/10.1016/j.theriogenology.2014.09.027.
[11] Y. H, L. J, L. J.R, L. J.Y, J. B.C, S. C.S, K. S.H, Optimal vitrification protocol forovarian tissue cryopreservation: the effect of cryoprotective agents and in vitro culture on vitrified-warmed ovarian tissue survival, Hum. Reprod. 28 (2013).
[12] J. Lee, H.S. Kong, E.J. Kim, H.W. Youm, J.R. Lee, C.S. Suh, S.H. Kim, Ovarian injury during cryopreservation and transplantation in mice: a comparative study between cryoinjury and ischemic injury, Hum. Reprod. 31 (2016) 1827–1837, https://doi.org/10.1093/humrep/dew144.
[13] H.W. Youm, J.R. Lee, J. Lee, B.C. Jee, C.S. Suh, S.H. Kim, Transplantation of mouse ovarian tissue: comparison of the transplantation sites, Theriogenology 83 (2015) 854–861, https://doi.org/10.1016/j.theriogenology.2014.11.026.
[14] D.D. Manavella, L. Cacciottola, C.M. Desmet, B.F. Jordan, J. Donnez, C.A. Amorim, M.M. Dolmans, Adipose tissue-derived stem cells in a fibrin implant enhance neovascularization in a peritoneal grafting site: a potential way to improve ovarian tissue transplantation, Hum. Reprod. 33 (2018) 270–279, https://doi.org/10.1093/humrep/dex374.
[15] L. Cacciottola, D.D. Manavella, C.A. Amorim, J. Donnez, M.-M. Dolmans, In vivo characterization of metabolic activity and oxidative stress in grafted human

ovarian tissue using microdialysis, Fertil. Steril. 110 (2018) 534–544.e3, https://doi.org/10.1016/j.fertnstert.2018.04.009.
[16] G. Rahimi, V. Isachenko, R. Kreienberg, H. Sauer, P. Todorov, S. Tawadros, P. Mallmann, F. Nawroth, E. Isachenko, Re-vascularisation in human ovarian tissue after conventional freezing or vitrification and xenotransplantation, Eur. J. Obstet. Gynecol. Reprod. Biol. 149 (2010) 63–67, https://doi.org/10.1016/j.ejogrb.2009.11.015.
[17] N.J. Donfack, K.A. Alves, V.R. Araújo, A. Cordova, J.R. Figueiredo, J. Smitz, A.P. R. Rodrigues, Expectations and limitations of ovarian tissue transplantation, Zygote 25 (2017) 391–403, https://doi.org/10.1017/S0967199417000338.
[18] A. Shikanov, Z. Zhang, M. Xu, R.M. Smith, A. Rajan, T.K. Woodruff, L.D. Shea, Fibrin encapsulation and vascular endothelial growth factor delivery promotes ovarian graft survival in mice, Tissue Eng Part A 17 (2011) 3095–3104, https://doi.org/10.1089/ten.tea.2011.0204.
[19] A. Tanaka, H. Nakamura, Y. Tabata, Y. Fujimori, K. Kumasawa, T. Kimura, Effect of sustained release of basic fibroblast growth factor using biodegradable gelatin hydrogels on frozen-thawed human ovarian tissue in a xenograft model, J. Obstet. Gynaecol. Res. (2018), https://doi.org/10.1111/jog.13726.
[20] H. Suzuki, T. Ishijima, S. Maruyama, Y. Yanagimoto Ueta, Y. Abe, H. Saitoh, Beneficial effect of desialylated erythropoietin administration on the frozen-thawed canine ovarian xenotransplantation, J. Assist. Reprod. Genet. 25 (2008) 571–575, https://doi.org/10.1007/s10815-008-9271-9.
[21] L. Commin, S. Buff, E. Rosset, C. Galet, A. Allard, P. Bruyere, T. Joly, P. Guérin, V. Neto, Follicle development in cryopreserved bitch ovarian tissue grafted to immunodeficient mouse, Reprod. Fertil. Dev. 24 (2012) 461, https://doi.org/10.1071/RD11166.
[22] R. Soleimani, E. Heytens, K. Oktay, Enhancement of neoangiogenesis and follicle survival by sphingosine-1-phosphate in human ovarian tissue xenotransplants, PLoS One 6 (2011) e19475, https://doi.org/10.1371/journal.pone.0019475.
[23] M. Saber, H. Eimani, M. Soleimani Mehranjani, A. Shahverdi, H.R. Momeni, R. Fathi, S. Tavana, The effect of Verapamil on ischaemia/reperfusion injury in mouse ovarian tissue transplantation, Biomed. Pharmacother. 108 (2018) 1313–1319, https://doi.org/10.1016/j.biopha.2018.09.130.
[24] M.-M. Dolmans, J. Donnez, L. Cacciottola, Fertility preservation: the challenge of freezing and transplanting ovarian tissue, Trends Mol. Med. 27 (2021) 777–791, https://doi.org/10.1016/j.molmed.2020.11.003.
[25] J. Callejo, C. Salvador, S. González-Nuñez, L. Almeida, L. Rodriguez, L. Marqués, A. Valls, J.M. Lailla, Live birth in a woman without ovaries after autograft of frozen-thawed ovarian tissue combined with growth factors, J. Ovarian Res. 6 (2013), https://doi.org/10.1186/1757-2215-6-33.
[26] J.R. Lee, H.W. Youm, S.K. Kim, B.C. Jee, C.S. Suh, S.H. Kim, Effect of necrostatin on mouse ovarian cryopreservation and transplantation, Eur. J. Obstet. Gynecol. Reprod. Biol. 178 (2014), https://doi.org/10.1016/j.ejogrb.2014.04.040.
[27] H.W. Youm, J. Lee, E.J. Kim, H.S. Kong, J.R. Lee, C.S. Suh, S.H. Kim, Effects of angiopoietin-2 on transplanted mouse ovarian tissue, PLoS One 11 (2016), https://doi.org/10.1371/journal.pone.0166782.
[28] C.E. Martínez, P.C. Smith, V.A. Palma Alvarado, The influence of platelet-derived products on angiogenesis and tissue repair: a concise update, Front. Physiol. 6 (2015), https://doi.org/10.3389/fphys.2015.00290.
[29] M. Raica, A.M. Cimpean, Platelet-derived growth factor (PDGF)/PDGF receptors (PDGFR) Axis as target for antitumor and antiangiogenic therapy, Pharmaceuticals 3 (2010) 572–599, https://doi.org/10.3390/ph3030572.
[30] H. Cheng, J. Zhang, J. Li, M. Jia, Y. Wang, H. Shen, Platelet-rich plasma stimulates angiogenesis in mice which may promote hair growth, Eur. J. Med. Res. 22 (2017), https://doi.org/10.1186/s40001-017-0278-5.
[31] M.C. Barsotti, P. Losi, E. Briganti, E. Sanguinetti, A. Magera, T. Al Kayal, R. Feriani, R. Di Stefano, G. Soldani, Effect of platelet lysate on human cells involved in different phases of wound healing, PLoS One 8 (2013), https://doi.org/10.1371/journal.pone.0084753.
[32] R. Alves, R. Grimalt, A review of platelet-rich plasma: history, biology, mechanism of action, and classification, Skin Appendage Disord. 4 (2018) 18–24, https://doi.org/10.1159/000477353.
[33] P. Everts, K. Onishi, P. Jayaram, J.F. Lana, K. Mautner, Platelet-rich plasma: new performance understandings and therapeutic considerations in 2020, Int. J. Mol. Sci. 21 (2020) 7794, https://doi.org/10.3390/ijms21207794.
[34] H.Y. Jang, S.M. Myoung, J.M. Choe, T. Kim, Y.P. Cheon, Y.M. Kim, H. Park, Effects of autologous platelet-rich plasma on regeneration of damaged endometrium in female rats, Yonsei Med. J. 58 (2017) 1195–1203, https://doi.org/10.3349/ymj.2017.58.6.1195.
[35] S.S. Anvari, G. Dehgan, M. Razi, Preliminary findings of platelet-rich plasma-induced ameliorative effect on polycystic ovarian syndrome, Cell J 21 (2019) 243–252, https://doi.org/10.22074/cellj.2019.5952.
[36] E. Scott Sills, S.H. Wood, Autologous activated platelet-rich plasma injection into adult human ovary tissue: molecular mechanism, analysis, and discussion of reproductive response, Biosci. Rep. 39 (2019), https://doi.org/10.1042/BSR20190805.
[37] K. Sfakianoudis, M. Simopoulou, N. Nitsos, L. Lazaros, A. Rapani, A. Pantou, M. Koutsilieris, Y. Nikas, K. Pantos, Successful implantation and live birth following autologous platelet-rich plasma treatment for a patient with recurrent implantation failure and chronic endometritis, In Vivo (Brooklyn) 33 (2019) 515–521, https://doi.org/10.21873/invivo.11504.
[38] F. Dehghani, H. Aboutalebi, T. Esmaeilpour, M.R. Panjehshahin, H. Bordbar, Effect of platelet-rich plasma (PRP) on ovarian structures in cyclophosphamide-induced ovarian failure in female rats: a stereological study, Toxicol. Mech. Methods 28 (2018) 653–659, https://doi.org/10.1080/15376516.2018.1491662.
[39] L. Nazari, S. Salehpour, S. Hoseini, S. Zadehmodarres, E. Azargashb, Effects of autologous platelet-rich plasma on endometrial expansion in patients undergoing frozen-thawed embryo transfer: a double-blind RCT, Int J Reprod Biomed 17 (2019) 445–450, https://doi.org/10.18502/ijrm.v17i6.4816.
[40] M. Farimani, S. Heshmati, J. Poorolajal, M. Bahmanzadeh, A report on three live births in women with poor ovarian response following intra-ovarian injection of platelet-rich plasma (PRP), Mol. Biol. Rep. 46 (2019) 1611–1616, https://doi.org/10.1007/s11033-019-04609-w.
[41] S. Seckin, H. Ramadan, M. Mouanness, M. Kohansieh, Z. Merhi, Ovarian response to intraovarian platelet-rich plasma (PRP) administration: hypotheses and potential mechanisms of action, J. Assist. Reprod. Genet. 39 (2022) 37–61, https://doi.org/10.1007/s10815-021-02385-w.
[42] R.I. Litvinov, J.W. Weisel, Fibrin mechanical properties and their structural origins, Matrix Biol. 60–61 (2017) 110–123, https://doi.org/10.1016/j.matbio.2016.08.003.
[43] A. Noori, S.J. Ashrafi, R. Vaez-Ghaemi, A. Hatamian-Zaremi, T.J. Webster, A review of fibrin and fibrin composites for bone tissue engineering, Int J Nanomedicine 12 (2017) 4937–4961, https://doi.org/10.2147/IJN.S124671.
[44] I.S. Bayer, Advances in fibrin-based materials in wound repair: a review, Molecules 27 (2022) 4504, https://doi.org/10.3390/molecules27144504.
[45] C. Yang, N. Chung, C. Song, H.W. Youm, K. Lee, J.R. Lee, Promotion of angiogenesis toward transplanted ovaries using nitric oxide releasing nanoparticles in fibrin hydrogel, Biofabrication 14 (2022), https://doi.org/10.1088/1758-5090/ac3f28.
[46] T. Toyoda, K. Isobe, T. Tsujino, Y. Koyata, F. Ohyagi, T. Watanabe, M. Nakamura, Y. Kitamura, H. Okudera, K. Nakata, T. Kawase, Direct activation of platelets by addition of CaCl2 leads coagulation of platelet-rich plasma, Int. J. Implant Dent. 4 (2018), https://doi.org/10.1186/s40729-018-0134-6.
[47] J. Etulain, H.A. Mena, R.P. Meiss, G. Frechtel, S. Gutt, S. Negrotto, M. Schattner, An optimised protocol for platelet-rich plasma preparation to improve its angiogenic and regenerative properties, Sci. Rep. 8 (2018), https://doi.org/10.1038/s41598-018-19419-6.
[48] H.W. Youm, J.R. Lee, J. Lee, B.C. Jee, C.S. Suh, S.H. Kim, Transplantation of mouse ovarian tissue: comparison of the transplantation sites, Theriogenology 83 (2015) 854–861, https://doi.org/10.1016/j.theriogenology.2014.11.026.
[49] T. Lundy, P. Smith, A. O'Connell, N.L. Hudson, K.P. McNatty, Populations of granulosa cells in small follicles of the sheep ovary, Reproduction 115 (1999) 251–262, https://doi.org/10.1530/jrf.0.1150251.
[50] R.E. Marx, Platelet-rich plasma (PRP): what is PRP and what is not PRP? Implant Dent. 10 (2001) 225–228, https://doi.org/10.1097/00008505-200110000-00002.
[51] S.P. Arnoczky, D. Delos, S.A. Rodeo, What is platelet-rich plasma? Oper Tech Sports Med 19 (2011) 142–148, https://doi.org/10.1053/J.OTSM.2010.12.001.
[52] Z. Tahergorabi, M. Khazaei, A Review on Angiogenesis and Its Assays, n.d. www.mums.ac.ir.
[53] R. Lugano, M. Ramachandran, A. Dimberg, Tumor angiogenesis: causes, consequences, challenges and opportunities, Cell. Mol. Life Sci. 77 (2020) 1745–1770, https://doi.org/10.1007/s00018-019-03351-7.
[54] W. Olejarz, G. Kubiak-Tomaszewska, A. Chrzanowska, T. Lorenc, Exosomes in angiogenesis and anti-angiogenic therapy in cancers, Int. J. Mol. Sci. 21 (2020) 1–25, https://doi.org/10.3390/ijms21165840.
[55] H. El-Sharkawy, A. Kantarci, J. Deady, H. Hasturk, H. Liu, M. Alshahat, T.E. Van Dyke, Platelet-rich plasma: growth factors and pro- and anti-inflammatory properties, J. Periodontol. 78 (2007) 661–669, https://doi.org/10.1902/jop.2007.060302.
[56] R.M. McFee, T.G. Rozell, A.S. Cupp, The balance of proangiogenic and antiangiogenic VEGFA isoforms regulate follicle development, Cell Tissue Res. 349 (2012) 635–647, https://doi.org/10.1007/s00441-012-1330-y.
[57] S. Ramanujan, G.C. Koenig, T.P. Padera, B.R. Stoll, R.K. Jain, Local imbalance of proangiogenic and antiangiogenic factors: a potential mechanism of focal necrosis and dormancy in tumors 1. http://aacrjournals.org/cancerres/article-pdf/60/5/1442/3241647/ch050001442p.pdf, 2000.
[58] E.A. Pollina, A. Legesse-Miller, E. Haley, T. Goodpaster, J. Randolph-Habecker, H. A. Coller, Regulating the angiogenic balance in tissues: a potential role for the proliferative state of fibroblasts, Cell Cycle 7 (2008) 2056–2070, https://doi.org/10.4161/cc.7.13.6240.
[59] M. Bisht, D. Dhasmana, S. Bist, Angiogenesis: future of pharmacological modulation, Indian J. Pharmacol. 42 (2010) 2, https://doi.org/10.4103/0253-7613.62395.
[60] B.L. Krock, N. Skuli, M.C. Simon, Hypoxia-induced angiogenesis: good and evil, Genes Cancer 2 (2011) 1117–1133, https://doi.org/10.1177/1947601911423654.
[61] N. DeWitt, Angiogenesis, Nature 438 (2005), https://doi.org/10.1038/438931a, 931–931.
[62] A.A. Ucuzian, A.A. Gassman, A.T. East, H.P. Greisler, Molecular mediators of angiogenesis, J. Burn Care Res. 31 (2010) 158–175, https://doi.org/10.1097/BCR.0b013e3181c7ed82.
[63] P. Nyberg, L. Xie, R. Kalluri, Endogenous Inhibitors of Angiogenesis, n.d. www.aacrjournals.org.
[64] H. Zhu, Y. Zhang, Y. Zhong, Y. Ye, X. Hu, L. Gu, X. Xiong, Inflammation-mediated angiogenesis in ischemic stroke, Front. Cell. Neurosci. 15 (2021), https://doi.org/10.3389/fncel.2021.652647.
[65] X. Chen, W. Yu, J. Zhang, X. Fan, X. Liu, Q. Liu, S. Pan, R.A.F. Dixon, P. Li, P. Yu, A. Shi, Therapeutic angiogenesis and tissue revascularization in ischemic vascular disease, J. Biol. Eng. 17 (2023), https://doi.org/10.1186/s13036-023-00330-2.
[66] J.M. Isner, T. Asahara, Angiogenesis and vasculogenesis as therapeutic strategies for postnatal neovascularization, J. Clin. Invest. 103 (1999) 1231–1236, https://doi.org/10.1172/JCI6889.

[67] M. Teichert, L. Milde, A. Holm, L. Stanicek, N. Gengenbacher, S. Savant, T. Ruckdeschel, Z. Hasanov, K. Srivastava, J. Hu, S. Hertel, A. Bartol, K. Schlereth, H.G. Augustin, Pericyte-expressed Tie2 controls angiogenesis and vessel maturation, Nat. Commun. 8 (2017), https://doi.org/10.1038/ncomms16106.
[68] E. Fahey, S.L. Doyle, IL-1 family cytokine regulation of vascular permeability and angiogenesis, Front. Immunol. 10 (2019), https://doi.org/10.3389/fimmu.2019.01426.
[69] R. Pasqualini, E. Koivunen, R. Kain, J. Lahdenranta, M. Sakamoto, A. Stryhn, R. A. Ashmun, L.H. Shapiro, W. Arap, E. Ruoslahti, Aminopeptidase N Is a Receptor for Tumor-Homing Peptides and a Target for Inhibiting Angiogenesis 1, 2000.
[70] K. Patra, S. Jana, A. Sarkar, D.P. Mandal, S. Bhattacharjee, The inhibition of hypoxia-induced angiogenesis and metastasis by cinnamaldehyde is mediated by decreasing HIF-1α protein synthesis via PI3K/Akt pathway, Biofactors 45 (2019) 401–415, https://doi.org/10.1002/biof.1499.
[71] T. Puidokas, M. Kubilius, D. Nomeika, G. Januzis, E. Skrodeniene, Comparative analysis of blood clot, plasma rich in growth factors and platelet-rich fibrin resistance to bacteria-induced fibrinolysis, Microorganisms 7 (2019), https://doi.org/10.3390/microorganisms7090328.
[72] A. Caruana, D. Savina, J.P. Macedo, S.C. Soares, From platelet-rich plasma to advanced platelet-rich fibrin: biological achievements and clinical advances in modern surgery, Eur J Dent 13 (2019) 280–286, https://doi.org/10.1055/s-0039-1696585.
[73] D.H. Alamdari, Mohamad, R. Motie, N. Kamalahmadi, M. Aliakbarian, Autologous Platelet-Rich Plasma and Fibrin Glue Decrease Pain Following Excision and Primary Closure of Pilonidal Sinus, 2019.
[74] D.M. Dohan, J. Choukroun, A. Diss, S.L. Dohan, A.J.J. Dohan, J. Mouhyi, B. Gogly, Platelet-rich fibrin (PRF): a second-generation platelet concentrate. Part I: technological concepts and evolution, Oral Surgery, Oral Medicine, Oral Pathology, Oral Radiology and Endodontology 101 (2006), https://doi.org/10.1016/j.tripleo.2005.07.008.
[75] K.C. Gersh, C. Nagaswami, J.W. Weisel, Fibrin network structure and clot mechanical properties are altered by incorporation of erythrocytes, Thromb Haemost 102 (2009) 1169–1175, https://doi.org/10.1160/TH09-03-0199.
[76] E. Anitua, M. Sánchez, A.T. Nurden, P. Nurden, G. Orive, I. Andía, New insights into and novel applications for platelet-rich fibrin therapies, Trends Biotechnol. 24 (2006) 227–234, https://doi.org/10.1016/j.tibtech.2006.02.010.
[77] J.W. Weisel, The Mechanical Properties of Fibrin for Basic Scientists and Clinicians, n.d.
[78] E. Lucarelli, R. Beretta, B. Dozza, P.L. Tazzari, S.M. O'Connell, F. Ricci, M. Pierini, S. Squarzoni, P.P. Pagliaro, E.I. Oprita, D. Donati, A recently developed bifacial platelet-rich fibrin matrix, Eur. Cell. Mater. 20 (2010) 13–23, https://doi.org/10.22203/eCM.v020a02.
[79] W. Zhu, Y.-W. Liu, L.-Z. Zhou, X.-S. Weng, Strategy of injectable hydrogel and its application in tissue engineering, Chin Med J (Engl). 134 (2020) 275–277, https://doi.org/10.1097/CM9.0000000000001055.
[80] B. Arjmand, P. Goodarzi, F. Mohamadi-Jahani, K. Falahzadeh, B. Larijani, Personalized regenerative medicine, Acta Med. Iran. 55 (2017) 144–149.
[81] G. Rozen, K. Stern, Surgical approach to heterotopic ovarian tissue transplantation, in: Principles and Practice of Ovarian Tissue Cryopreservation and Transplantation, Elsevier, 2022, pp. 169–175, https://doi.org/10.1016/B978-0-12-823344-3.00026-1.
[82] D.R. Senger, G.E. Davis, Angiogenesis, Cold Spring Harb Perspect Biol 3 (2011), https://doi.org/10.1101/cshperspect.a005090 a005090–a005090.
[83] H. Zhu, Y. Zhang, Y. Zhong, Y. Ye, X. Hu, L. Gu, X. Xiong, Inflammation-mediated angiogenesis in ischemic stroke, Front. Cell. Neurosci. 15 (2021), https://doi.org/10.3389/fncel.2021.652647.
[84] W.X. Zong, C.B. Thompson, Necrotic death as a cell fate, Genes Dev. 20 (2006) 1–15, https://doi.org/10.1101/gad.1376506.
[85] C.L. Moore, A.V. Savenka, A.G. Basnakian, TUNEL assay: a powerful tool for kidney injury evaluation, Int. J. Mol. Sci. 22 (1) (2021 Jan 2) 412, https://doi.org/10.3390/ijms22010412. PMID: 33401733; PMCID: PMC7795088.
[86] M. Weber, D. Bellwald, C. Wingenfeld, A. Hempfing, M. Leunig, The avascular talus: revascularization in an animal model, Foot Ankle Int. 25 (3) (2004) 151–158, https://doi.org/10.1177/107110070402500308.
[87] Arup Das, Paul G. McGuire, Retinal and choroidal angiogenesis: pathophysiology and strategies for inhibition, Prog. Retin. Eye Res. (2003) 721–748, https://doi.org/10.1016/j.preteyeres.2003.08.001. ISSN 1350-9462.
[88] G.E. Davis, D.R. Senger, Extracellular matrix mediates a molecular balance between vascular morphogenesis and regression, Curr. Opin. Hematol. 15 (2008) 197–203, https://doi.org/10.1097/MOH.0b013e3282fcc321.
[89] Y. Li, M. Chopp, N. Jiang, Z.G. Zhang, C. Zaloga, Induction of DNA fragmentation after 10 to 120 minutes of focal cerebral ischemia in rats, Stroke 26 (1995) 1252–1258, https://doi.org/10.1161/01.STR.26.7.1252.
[90] S.L. Tan, J. Zaidi, S. Campbell, P. Doyle, W. Collins, Blood flow changes in the ovarian and uterine arteries during the normal menstrual cycle, Am. J. Obstet. Gynecol. 175 (1996) 625–631, https://doi.org/10.1053/ob.1996.v175.a73865.
[91] R. Donnelly, J.M.C. Yeung, Therapeutic angiogenesis: a step forward in intermittent claudication, Lancet 359 (2002) 2048–2050, https://doi.org/10.1016/S0140-6736(02)08946-8.
[92] J.-C. Wang, G.-Y. Li, P.-P. Li, X. Sun, W.-M. Li, Y. Li, S.-Y. Lu, P.-J. Liu, Suppression of hypoxia-induced excessive angiogenesis by metformin via elevating tumor blood perfusion, Oncotarget 8 (2017) 73892–73904, https://doi.org/10.18632/oncotarget.18029.
[93] P. Madeddu, Therapeutic angiogenesis and vasculogenesis for tissue regeneration, Exp. Physiol. 90 (2005) 315–326, https://doi.org/10.1113/expphysiol.2004.028571.
[94] F. Danielsson, M. Skogs, M. Huss, E. Rexhepaj, G. O'Hurley, D. Klevebring, F. Pontén, A.K.B. Gad, M. Uhlén, E. Lundberg, Majority of differentially expressed genes are down-regulated during malignant transformation in a four-stage model, Proc Natl Acad Sci U S A. 110 (2013) 6853–6858, https://doi.org/10.1073/pnas.1216436110.